frontiers | Frontiers in Materials

TYPE Review
PUBLISHED 30 November 2023
DOI 10.3389/fmats.2023.1241869

OPEN ACCESS

EDITED BY
Behzad Nematollahi,
Swinburne University of Technology, Australia

REVIEWED BY
Seyed Ghaffar,
Brunel University London, United Kingdom
Kinga Korniejenko,
Cracow University of Technology, Poland
Pshtiwan Shakor,
Sulaimani Polytechnic University, Iraq
Mehdi Chougan,
Brunel University London, United Kingdom

*CORRESPONDENCE
Alireza Bahrami,
alireza.bahrami@hig.se
Santosh Shah,
sgshah.civil@spcevng.ac.in

RECEIVED 17 June 2023
ACCEPTED 18 October 2023
PUBLISHED 30 November 2023

CITATION
Barve P, Bahrami A and Shah S (2023), Geopolymer 3D printing: a comprehensive review on rheological and structural performance assessment, printing process parameters, and microstructure.
Front. Mater. 10:1241869.
doi: 10.3389/fmats.2023.1241869

Geopolymer 3D printing: a comprehensive review on rheological and structural performance assessment, printing process parameters, and microstructure

Prasad Barve[1], Alireza Bahrami[2]* and Santosh Shah[3]*

[1]Gujarat Technological University, Ahmedabad, India, [2]Department of Building Engineering, Energy Systems and Sustainability Science, Faculty of Engineering and Sustainable Development, University of Gävle, Gävle, Sweden, [3]Civil Engineering Department, Sankalchand Patel College of Engineering, Sankalchand Patel University, Visnagar, India

Geopolymers are under scrutiny as a sustainable alternative to cement in 3D printing for eco-friendly construction. Geopolymer 3D printing (G3DP) holds promise for green construction and advanced manufacturing. This study addresses G3DP's rheological properties, printability, and microstructure analysis. Results indicate the pivotal role of the rheological properties in the printability, encompassing parameters like the pumpability, extrudability, and shape retention. Lower viscosity and appropriate yield stress are crucial. The structural performance of G3DP, given its inherent anisotropic nature and assessment techniques, is scrutinized. Process variables such as nozzle design and print speed and interval affect the printability, buildability, and structural properties. Research on the parameters' optimization is necessary. Additionally, evaluation techniques for the G3DP's rheological and structural behaviors require standardization. Understanding the G3DP's rheology is paramount for the successful 3D printing construction. Findings offer quantitative insights into the importance of the rheological properties for the printability and structural performance. The microstructural analysis uncovers the porosity and density disparities compared to traditional geopolymers. This comprehensive review provides valuable insights for researchers and practitioners to enhance the G3DP's application as a futuristic sustainable construction material.

KEYWORDS

3D printed concrete, geopolymer, rheological properties, structural properties, testing method, assessment approach, microstructure

1 Introduction

Enhancing the efficiency of building work is the fundamental motivation for the development of 3D printing or additive manufacturing technology (Buswell et al., 2007). In order to solve industry concerns including labor skills, safety, and design complexity while realizing the promise for new processes and materials in construction, innovation in construction technology is required, particularly through rapid manufacturing and freeform construction (Buswell et al., 2007). Large-scale additive manufacturing

processes are now being used in the construction industry, which highlights the advantages of 3D printing concrete but also raises issues with material sensitivity and site conditions (Lim et al., 2012). This suggests that factory-based production of significant components is in line with industry trends toward better quality, speed, and safety (Lim et al., 2012). By lowering labor costs and material waste, the expanding usage of 3D printing in construction has the potential to revolutionize current building practices (Tay et al., 2017). With an emphasis on expanding the range of materials that can be printed, improving cost-effectiveness and minimizing environmental impact through design optimization and sophisticated control systems, the future of concrete 3D printing depends on overcoming technical obstacles, financial implications, and environmental benefits (De Schutter et al., 2018). Along with the importance of material formulations, there is a multidisciplinary importance of materials science, architecture, computation, and robotics in advancing additive manufacturing for the construction industry (Ghaffar et al., 2018). It is important to note that understanding material properties, optimizing mix designs, and ensuring robust configurations for additive manufacturing processes are prerequisites for the industry-changing, eco-innovative, and time-saving additive manufacturing processes (Ghaffar et al., 2018). While digital fabrication with concrete has the potential to revolutionize construction through lower costs, sustainability, and increased functionality, interdisciplinary research is required to address a number of technical issues, such as material formulations and processing-performance relationships (Wangler et al., 2019). These issues are equally important to address in order to advance this technology, along with sustainability, functionality, creativity, and interdisciplinarity (Wangler et al., 2019).

Additive manufacturing in construction is becoming increasingly popular throughout the world in both the building industry and the scientific community as a new era of Industry 4.0 dawns (Labonnote et al., 2016), despite its relatively modest rate of development in comparison to other industries. Even though 3D printing has uses in a various fields, such as biomedical and aerospace industries, its capacity for customization and complexity in building while addressing problems like void formation, anisotropic behavior, and material limitations may lead to its wider adoption (Ngo et al., 2018). In the context of the ongoing digital transformation of the construction industry (Construction 4.0), improved printing processes, novel materials, multi-material deposition, adherence to construction standards, and collaboration with other technologies like the integration of smart materials and sensors are required for optimizing material components and evaluating additive manufacturing's economic viability (Craveiroa et al., 2019). For large-scale on-site concrete construction, the CONPrint3D concept focuses on adaptability to modern architectural and structural design, the use of existing construction equipment, compliance with concrete standards, and specialized printheads for precise surface quality and geometric accuracy (Mechtcherine et al., 2019). Construction technologies like contour crafting, concrete printing, and d-shape, as well as potential applications like recycling construction waste, building complex structures, affordable housing, military bunkers, space exploration, building on the moon and Mars, and even repairing damaged structures, are all gaining popularity (Zhang et al., 2019).

Contour crafting, developed in the mid-1990s, was the first fused deposition modeling-based additive manufacturing method in construction (Khoshnevis et al., 2006; Khan et al., 2020; Mohan et al., 2021a). Eventually, stereolithography-inspired particle bed printing emerged, in which the binder liquid is selectively deposited into the powder bed to bond the powder grains (Cesaretti et al., 2014; Mohan et al., 2021a). Extrusion-based 3D printing uses 3D printers and powerful robotic arms to deposit contents layer after layer to fabricate the required structure from a digitally planned design, utilizing an automated method and slicing tools that output a G-code for each layer (Khoshnevis, 2004; Buswell et al., 2018; Shakor et al., 2019b; Khan et al., 2020). About 15%–45% of the overall mix fraction of most 3D-printed concrete is composed of Portland cement (Zhang et al., 2021). Since the process of extrusion is obstructed with the use of coarse aggregates in print ink, the binder and fine aggregate amount are exceptionally greater in concrete 3D printing of cementitious materials (Mohan et al., 2021b). Since Portland cement manufacturing accounts for about 6%–9% of worldwide carbon dioxide emissions (Santos and Cilla, 2022), the increased use of Portland cement may contribute to increased material expenses and decreased sustainability. Geopolymers are the reaction products formed when aluminosilicate sources are alkali activated to synthesize into an inorganic polymer (Wang et al., 2019; Meng et al., 2021; Tay and Norkhairunnisa, 2021; Lao et al., 2023). Compared to ordinary Portland cement (OPC), geopolymer demonstrates a number of sustainability benefits. Firstly, because geopolymer production relies on aluminosilicate minerals and industrial waste, it generates much less carbon dioxide than cement production because of this. This makes it a more environmentally friendly option, aligning with global efforts to mitigate climate change. Secondly, geopolymer can make use of locally accessible resources, cutting down on travel time and energy use. By reducing the adverse effects of material sourcing on the environment, this encourages regional sustainability. Additionally, geopolymer-based buildings frequently display increased durability and tolerance to harsh environmental factors, resulting in longer service lives and lower maintenance needs. This material's resilience not only contributes to the sustainability of the material but also makes it a suitable candidate for high-performance applications like thin white-topping pavement, which must withstand heavy traffic loads and weathering (Sathvik et al., 2023). Regarding the use of sodium hydroxide (NaOH) as an alkaline activator in geopolymer production, it is essential to acknowledge that while this chemical is involved, its use is generally within controlled industrial settings. Safety protocols are in place to handle NaOH safely, and it is crucial to ensure that these protocols are followed rigorously during geopolymer production. 'Just-add-water' or 'one-part' geopolymer mixture formulations incorporating a small amount of sodium-based activator powder may be adopted instead of handling large volumes of viscous alkaline solutions (Bong et al., 2021). Moreover, research and development in the field of geopolymers are essential, with a focus on finding more sustainable alternatives to alkaline activators like NaOH. Efforts should be made to explore environmentally friendly substitutes, which may reduce safety concerns associated with sodium hydroxide. Thus, while geopolymer does involve the use of certain chemicals like NaOH, its sustainability arises from its lower carbon footprint and potential for local material sourcing when compared to OPC. Researchers and industry experts need to work actively on addressing safety concerns and finding more eco-friendly alternatives for alkaline activators,

further enhancing the sustainability of geopolymer technology. As a result, there has been some recent research focusing on the viability of employing geopolymer, a greener binder (Duxson et al., 2007; Neupane, 2016; Luukkonen et al., 2018; Gao et al., 2021; Zhao et al., 2021; Nagaraju et al., 2023), to build sustainable 3D printed concrete using either extrusion-based (Panda et al., 2017a; Nematollahi et al., 2019b; Bong et al., 2021) or particle bed (Nematollahi et al., 2019a; Xia et al., 2019; Elsayed et al., 2022) printing methods. Geopolymer 3D printing (G3DP) has its advantages and challenges. This article focuses on the extrusion technique, which is more suitable for G3DP than particle-bed printing. Sophisticated printable geopolymer products and materials have been examined by various researchers in terms of their potential applications in a variety of fields, such as producing conductive nanocomposites using graphene oxide nanosheets (Zhong et al., 2017; Zhou et al., 2020), artificial reefs creation (Ly et al., 2021), lightweight short carbon fiber G3DP Bouligand architecture structure with high toughness and strength (Ma et al., 2021), high temperature-sensing repair materials (Vlachakis et al., 2020), thermally efficient foams (Alghamdi and Neithalath, 2019), water treatment filters (Luukkonen et al., 2020), photocatalysts for methylene blue removal (Liu et al., 2023), self-healing and thermally stable 3D printed diamond/geopolymer composites (Tang and Tang, 2022), adsorbents with high porosity (Gonçalves et al., 2023; Ma et al., 2023), thermal processing of ion-exchanged 3D printed geopolymer resulting in the creation of monoclinic-celsian ceramic (Fu et al., 2019), and microwave absorption (Li et al., 2022).

Due to many distinctive qualities and attributes of geopolymers, 3D printing of geopolymers can be more challenging than 3D printing of conventional concrete or mortar. The viscosity of geopolymers is often lower than that of conventional concrete or mortar. The pumpability and extrudability benefits of this lower viscosity can outweigh the difficulties in retaining form and ensuring precise layer deposition during printing. It can be more difficult to control the flow of lower viscosity materials since excessive spreading and shape deformation must be avoided by fine-tuning the rheological parameters. Due to the chemical activation method used in geopolymers, they frequently set more quickly than conventional concrete or mortar. The open time for printing may be lowered with this quick setting. Throughout the printing process, it becomes essential to maintain the desired workability and consistency. Contrarily, typical concrete/mortar frequently has a longer open period, providing more flexibility during printing. Chemical reactions involving alkali activators and source materials like fly ash or metakaolin cause geopolymers to cure. The humidity and temperature of the surroundings can have an impact on this chemical cure. As geopolymers may need specialized curing protocols to prevent early curing or delayed strength development, achieving consistent curing conditions in the 3D printing environment can be more difficult compared to conventional concrete or mortar. The development of covalent bonds gives geopolymers a tendency to have strong interlayer bond relative to conventional concrete or mortar, but it can be challenging to maintain optimal layer adhesion without delamination or breaking. To achieve a strong and continuous bond between layers, controlling the printing process parameters such as print speed and print time interval becomes essential. Geopolymers can be more sensitive to variations in material composition and mixing procedures. Precise control over the feedstock materials, mixing ratios, and activator concentrations is essential to ensure consistent printability and performance. In contrast, traditional concrete or mortar may be more forgiving in terms of material variations. To accommodate their lower viscosity and rapid setting behavior, geopolymer-based inks can need unique nozzle designs and adjustments. It can be difficult to build the nozzle optimally to provide constant extrusion while avoiding nozzle blockage. In comparison to the more widely accessible concrete and mortar components, the availability of geopolymers and their source materials may vary locally, potentially limiting their wider acceptance for 3D printing. Therefore, while geopolymers can be 3D printed with benefits like high strength and durability, these materials' special characteristics such as lower viscosity, quick setting, and curing mechanisms present difficulties for accurate control, handling of the material, and maintaining shape and structural integrity throughout the printing process. In-depth knowledge of geopolymer materials and thorough optimization of printing processes are necessary to overcome these obstacles.

G3DP is fundamentally characterized by the ingredients (raw materials) and ingredient properties and their design mix to fulfil the rheological essentials of printability, i.e., the mixture's buildability, extrudability, and pumpability. Previously conducted studies have commented on the mixture components and material design of cementitious materials and its influence on the properties of 3D printed concrete (Ma and Wang, 2018; Wangler et al., 2019; Khan, 2020; Nair et al., 2020; Yang et al., 2020; Mohan et al., 2021a; Baduge et al., 2021; Rehman and Kim, 2021; Zhang et al., 2021; Al-Noaimat et al., 2022). For concrete 3D printing, the mix design poses a formidable challenge (Siddika et al., 2020). The mixture composition comprising precursors, alkali activators, aggregates, fibers, additives, and curing regimes affects the fresh and hardened behavior of G3DP (Bhattacherjee et al., 2021; Zhang et al., 2021). A careful design mix is needed to enhance its performance. Due to their availability, aluminosilicate precursors, such as fly ash and ground granulated blast furnace slag (GGBS), are commonly used as primary binders. Fly ash increases flowability, while GGBS can change the setting time and strength. Due to greater CaO levels, adding more GGBS to the mixture decreases flowability and workability. This results in the production of gel components (such as silica-aluminate and C-S-H structures) during early geopolymerization, which helps with layer retention (Xie et al., 2019). Angular GGBS particles improve paste cohesiveness by further reducing lubrication (Alghamdi et al., 2019). As a result of the spherical fly ash particles and the lubricating qualities of the alkaline activator, greater fly ash levels improve slump flow diameter, ensuring sufficient flowability in geopolymers (Deb et al., 2014). Increasing FA dosage prolongs the setting time. This is because higher CaO levels in the mixture affect geopolymers' setting time, and FA contains less CaO, causing a slower reaction (Humad et al., 2019). Conversely, adding GGBS accelerates the setting time due to its higher CaO content, which speeds up the hydration reaction in the mixture (Deb et al., 2014; Cao et al., 2018). Researchers have experimented with different combinations to optimize properties for 3D printing. Alkali activators, mainly sodium and potassium-based, activate the geopolymerization process. The molar ratios of various components affect properties like the setting time and compressive strength. Additives, including Sodium carboxymethyl cellulose (CMC), nano-clay, and superplasticizers, are incorporated to tailor rheological and

structural properties. Fine aggregates like river sand are commonly used for good shape retention and buildability. Curing conditions, such as temperature and humidity, affect the properties of G3DP. The influence of reinforcing elements on the properties of G3DP has been extensively studied in the literature. Different types of fibers, such as polyvinyl alcohol (PVA), polypropylene (PP), steel, carbon, and others, have been used to enhance the flexural, tensile, and interlayer bond strengths. Adding fibers during stacking can modify the bond strength, but an uneven surface may hinder layer adhesion, especially with steel fibers (Al-Qutaifi et al., 2018). The strength in compression perpendicular to the printing direction increased from 22 MPa to 36 MPa with the volume of PP fibers up to 0.25%, beyond which the compressive and interlayer bond strengths decreased (Nematollahi et al., 2018a). PVA fibers caused the least loss in the interlayer bond strength, while polyphenylene benzobisoxazol (PBO) fibers improved the flexural strength (Nematollahi et al., 2019b). A study (Shakor et al., 2020b) investigated the impact of E6-glass fiber in 3D printed mortar and found significant strength gains (108% in the compressive strength and 68% in the flexural strength) with just 1% more glass fiber. Approximately 80% of the fibers lined up with the orientation of the nozzle, and void research revealed gaps that were 6,000 μm wide and 1700 μm deep. On the surface, there were also visible tiny pores and voids. Thus, glass fibers improve mechanical qualities, and knowledge of fiber orientation and voids helps optimize 3D printed mortar for use in the building industry. To forecast the compressive and flexural strengths of 3D printed fiber-reinforced concrete (3DP-FRC), a study (Uddin et al., 2023) used six machine learning algorithms. Performance was good for XGBoost, LightGBM, and CatBoost, with XGBoost leading in terms of the flexural strength. The water/binder ratio, loading direction, and fiber volume percent were significant influencing factors for the compressive and flexural strengths. The relative importance of input variables was revealed by Shapley additive explanations (SHAP) analysis. Despite the data limitations, the study pointed out the potential for controlled experiments, enlarged databases, and a toolkit for 3DP-FRC mixture prediction. Studies have also explored the combination of fibers and steel micro-cables to increase the flexibility and strength in geopolymer composites (Lim et al., 2018; Ma et al., 2019; Li et al., 2020). Thus, the literature shows that including reinforcing elements, such as fibers and steel micro-cables, can significantly improve the mechanical properties of G3DP. A group of researchers evaluated the use of modified powder (CP) in construction powder-based 3D printing, emphasizing the advantages of heat curing at 80 °C to improve the compressive and flexural strengths in cubic mortar specimens (Shakor et al., 2023). They also assessed the possibility of using chopped glass fibers in reinforced mortar to show increased mechanical qualities. To highlight the anisotropic character of powder-based 3D printing, they studied how the orientation angles affect the mechanical behavior of specimens that have been 3D printed. The recommended orientation angles for different mechanical parameters ranged from 0° for the CP specimens' compressive and flexural strengths to 45° for the shear strength. For the compression, shear, tension, and bending, commercial powder (ZP 151) specimens performed best at various orientation angles. Investigating the possibility of replacing conventional gypsum powder with custom-made cement mortar powder for powder-based 3D printing, the study (Shakor et al., 2020a) revealed that heat-curing and the addition of E6-glass fibers improve the mechanical characteristics and surface quality of printed cement mortar sample, where the highest compressive strength was attained by heat-curing at an optimal temperature of 80°C. In 3D printing, fresh concrete is prone to shrinkage cracking due to self-desiccation when microwave heating is adopted (Muthukrishnan et al., 2020). Still, the inclusion of micro PVA fibers can help mitigate this issue. Fiber incorporation affects the workability of the mix, and different fiber types have varying effects. Additionally, the careful selection of geopolymer components and additives is essential for achieving the desired workability, strength, and print quality in 3D-printed geopolymers. Furthermore, pretreatment measures may be necessary to improve micro-reinforcement impact.

Further, the existing studies (Korniejenko et al., 2022a; Korniejenko et al., 2022b) reviewing the microstructure of G3DP in the literature, which is essential to realize its reaction mechanism, are limited.

To conduct the literature search, the authors used a variety of keyword combinations pertaining to the 3D printing of geopolymers and additive manufacturing of geopolymers in construction, including "geopolymer 3D printing", "3D printing of geopolymers", "3D printing of alkali activated materials", "sustainable construction materials in 3D printing", and "geopolymer additive manufacturing". As the article focuses on the rheological and structural properties of G3DP, printing process variables, and microstructure of G3DP, the papers that did not match the scope were omitted from the review. The experimental data gathered from the literature is analyzed and presented in a tabular format. Researchers investigating the topic of G3DP will benefit from examining the most recent research trends and findings, which will also offer suggestions for future research directions.

The novelty of this research lies in its in-depth exploration of the rheological properties, printability characteristics, and microstructural analysis of G3DP materials. Considering various criteria, such as apparent viscosity, static yield stress, structural integrity, slump, spread diameter, green strength, and dimensional consistency, this article summarises the critical properties required for successful 3D printing. Additionally, this work investigates the microstructural analysis of G3DP materials using advanced techniques. These analyses provide crucial insights into the morphology, structural bond, voids, cracks, fracture bridging mechanisms, and porosity of G3DP materials. The conclusions drawn from this work will help researchers and practitioners optimize the parameters and develop strategies to enhance the structural properties, printability, and overall performance of G3DP materials.

2 Rheological assessment and performance of G3DP

Plastic viscosity and yield stress are two essential properties defining fresh geopolymer mixtures' rheological properties. The main rheological parameters relevant to 3D concrete printing material can be identified as the yield stress, viscosity, and thixotropy. The yield stress (τ_0) can be defined as the minimum shear stress at the onset of material flow (Jayathilakage et al., 2022). Below the yield stress limit, the material can exhibit solid-like behavior. The material can flow after exceeding the yield stress (Jayathilakage et al., 2022). Adhesion and surface roughness between

particles in the fresh mixture contribute to the mixture's inability to overcome the frictional force and develop plastic flow, which results in the yield stress (Sun et al., 2020). There are two types of the yield stress: static and dynamic. Static stress is the highest stress at which a substance initiates the flow, whereas dynamic stress is the lowest stress required to keep it flowing (Paul et al., 2018). Suppose one considers concrete as a fluid with infinite layers divided parallel to the flow direction. In that case, the resistance between the infinite fluid layers can be defined as the viscosity (μ) (Jayathilakage et al., 2022). The higher the material viscosity, the lower the flowability. The fresh mixture's internal structure hinders the flow because of its plastic viscosity. The fresh mixture's cohesiveness can be expressed by its plastic viscosity. Greater plastic viscosity makes the mixture more resilient when sheared (Sun et al., 2020). The shear stress increase is indicated by the plastic viscosity as the rate of the shear increases (Paul et al., 2018). Recovery of the viscosity is a measure of a material's adaptability to different shear speeds (Panda and Tan, 2019). Before the final setting, the stiffening rate of the material can be gauged by the pace at which structural build-up occurs (Panda and Tan, 2019). Static stresses are distinguished from dynamic stresses by the material's thixotropy. When the shear rate or shear stress is raised, a fluid's viscosity decreases reversibly, isothermally, and over time, referred to as thixotropy (Panda et al., 2018b). To achieve G3DP quality, the material must be able to flow and can be extruded out of a nozzle, adhere to the preceding layer, and hold its dimensions under growing stress caused by the buildup of subsequent layers. Regarding the G3DP's printability, the rheological characteristics of the printable ink are directly linked to its quality. A print mix's pumpability relates to how well it can be pumped to a printer under pressure and retain its original properties, in relation to printing. 3D concrete printing necessitates an extruded material that is relatively stiff to ascertain that the geometry of the extrudes remains unaltered after being pumped. High-density geopolymer mixes must have a balanced mix design that takes both the density and flowability into account to achieve the pumpability. Superplasticizers and other additives can lessen the viscosity, improving flow, and reducing obstructions. Handling highly viscous materials requires a careful selection of pumps, such as piston or peristaltic pumps. Preserving the pumpability requires precise temperature control during printing to prevent premature setting. For low-density geopolymer mixes, air-entraining agents and lightweight aggregates are essential for enhancing pumpability. Pumpability is ensured without sacrificing stability through the regulation of the viscosity through mix design modifications. To match flow rate and pressure with material characteristics, equipment settings must be calibrated. Extrudability refers to the characteristic of a material that can be printed, leading to a continuous layer from the extruder, enabling an uninterrupted discharge of material (Le et al., 2012a; Lim et al., 2012; Roussel, 2018; Şahin et al., 2021). Extruding as bonded layers from the nozzle, the print material's buildability is what determines how well it can bear the overloaded weight of future layers produced by the printing process (Perrot et al., 2016; Wangler et al., 2016; Roussel, 2018). Another crucial aspect of 3D printing is open time, that is the period during which the mix must be extruded (Lim et al., 2012; Wangler et al., 2016). Material can no longer be printed after its open period.

Geopolymer-based concrete and traditional concrete demonstrate distinct variances in their thixotropic behaviors when used in 3D printing. Due to its increased viscosity, conventional concrete might be difficult to extrude through 3D printing nozzles. It might, therefore, necessitate slower printing speeds and more exact management of the printing parameters. Despite some thixotropic behavior in typical concrete, it is often minimal. It frequently takes a long time to recover after shearing, which might compromise the stability and accuracy of 3D printing procedures. The necessity for meticulous supervision and adjusting of the parameters of traditional concrete during 3D printing can result in lengthier printing periods and more complicated construction procedures. Superior thixotropic qualities in geopolymer-based concrete can help it self-level and flow more easily. This trait is beneficial for 3D printing, as maintaining a steady flow is necessary for accurate layer deposition. Geopolymers' improved thixotropic properties allow for faster 3D printing, shortening the construction process and improving the overall productivity. Concrete made from geopolymers often has less viscosity, which makes it simpler to extrude through printing nozzles. This characteristic facilitates smoother printing processes.

In the context of concrete rheology, two crucial behaviors are shear thinning and shear thickening. Shear thinning (pseudoplastic behavior), often observed in self-compacting concrete (SCC) when the water-to-cement (w/c) ratio exceeds 0.4, is characterized by a decrease in apparent viscosity as the shear rate increases (Gowripalan et al., 2021). Thus, when SCC experiences higher shear rates (e.g., during flow or placement), it becomes less viscous and flows more easily. This property is essential for SCC's self-leveling and flowable characteristics, making it suitable for various construction applications. On the other hand, shear thickening is a behavior where the viscosity of a material increases as the shear rate rises. While this is not typically observed in SCC, it is essential to understand, especially in other concrete types. Concrete can become less workable in scenarios with shear thickening, making it challenging to flow and place. This behavior is more common in non-fluid concrete mixtures. Understanding these rheological behaviors is essential for tailoring concrete mix designs to 3D printed construction needs and predicting how concrete will behave during placement, affecting factors like printability and workability.

Concrete is commonly considered a Bingham fluid (Bingham, 1922) with the yield stress and viscosity.

Consequently, as shown in Figure 1, the Bingham model (Bingham, 1922) is used to define the shear stress versus the shear strain behavior as:

$$\tau = \tau_0 + \mu \cdot \gamma \tag{1}$$

where τ is the shear stress and γ is the shear rate.

However, as mentioned earlier, concrete typically shows a thixotropic and shear-thinning behavior (i.e., the viscosity will reduce with the increasing shear rate). Therefore, as seen in Figure 1, to display the shear thinning behavior of concrete, the Herschel–Bulkley model (Herschel, 1924) is commonly used as:

$$\tau = \tau_0 + \mu \cdot \gamma^n \tag{2}$$

where n is the flow index and the value is usually lower than 1 for shear thinning fluids (n = 1 for Bingham fluids).

G3DP printing requires a high degree of printability. The printability demanded by G3DP is more sophisticated than

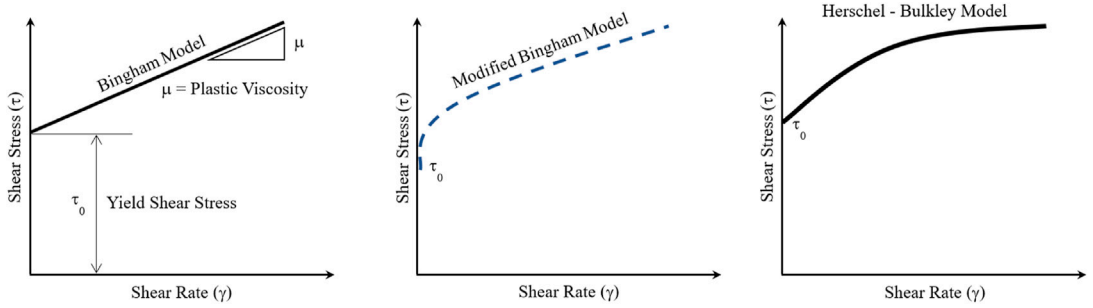

FIGURE 1
Rheological models used to realize rheological behavior of G3DP.

standard concrete workability. Thus, most standard concrete testing measurements turn out to be ineffective. G3DP's new metrics for assessing printability are, however, limited. Rheological assays, which may assess printability using a variety of rheological characteristics, are frequently used in research in this situation. Table 1 presents testing equipment and procedures various researchers adopt for determining rheological characteristics, i.e., the viscosity and yield stress of G3DP.

The devices attempting to use fluid rheology methods to measure the concrete flow by measuring the shear stress at varying shear rates are called rheometers (Hackley and Ferraris, 2001). The resistance to flow with varying shearing rates can be measured in the commercially available rheometers. They are high-precision, continuously-variable shear instruments in which the test fluid is sheared between rotating cylinders, cones, or plates, under controlled-stress or controlled-rate conditions. In accordance with Table 1, the static yield stress and average apparent viscosity of G3DP can be measured by employing a constant shear rate test, in which the material is sheared at a constant rate, and the material response peak to this constant shear rate is noted to determine the static yield stress. It is worth noting that a very high pre-shear is applied before performing the constant shear rate test to put the sample back to its reference state by eliminating the shear history. The ramp-up and ramp-down shear rate protocol measures the plastic viscosity and dynamic yield stress by fitting the Bingham model's response data. Respond fittings other than the Bingham model can be used for shear thinning materials such as Herschel-Bulkley, Power law, Cross, Carreau, Sisko, and Casson. Moreover, shear thinning and viscosity recovery protocol, which mimics the 3D printing stages, i.e., before extrusion (low shear rate), during extrusion (high shear rate), and after extrusion (low shear rate), is employed to understand the thixotropy behavior of the material. Thus, it can be concluded from Table 1 that the values of the viscosity and yield stress of G3DP for the pumpability, shape retention, and buildability properties rely on the test equipment utilized and the procedure adopted.

Figure 2 presents the flow chart for the rheology assessment of G3DP, including all types of testing. Table 2 presents different assessment approaches adopted for evaluating the printability characteristics, i.e., pumpability, extrudability, buildability, open time, and shape retention ability of G3DP.

Based on Table 2, properties such as the viscosity, structural integrity, yield stress, green strength, and elasticity are adopted as acceptance criteria for assessing the printability characteristics of G3DP. The mix design of G3DP oscillates between the challenging rheological demands of pumpability, extrudability, buildability, open time, and shape retention ability. The pumpability of G3DP is estimated using the plastic viscosity and dynamic yield stress, which shall, in turn, govern the pump pressure. A desirably suitable pumpability can be achieved with lower plastic viscosity and dynamic yield stress.

The viscosity, yield stress, and flowing ability govern the extrudability of G3DP (Table 2). The flowability is estimated through an optimum initial setting time, slump, and spread diameter. A harsh mix can lead to choking or blockage of the material inside the printer. The dynamic yield stress must be higher to achieve good extrudability since it is required to enable a continuous flow of material through the printhead. The optimum range of the static yield stress for proper extrudability is mentioned in Table 2. The greater the specified rebuilding energy, the better the extrudability will be. Sometimes, property like extrudability is analyzed through visual inspection due to the unavailability of a standard procedure for its assessment. Moreover, manual observations lack precision and are thus less reliable in quantifying the printing process.

The open time of G3DP is associated with the initial setting time, static yield stress, and printing disruption time (Table 2). Material can no longer be printed after its open period. It is also observed from Table 2 that an excellent buildability of G3DP is linked to high viscosity recovery ability, higher green strength of the material, lesser nozzle stand-off distance, good slump retention, higher elastic modulus, high rate of increase in the static yield stress, and no or minimum visible distortion of the bottom layer as well as an entire printed product, i.e., good structural integrity, which enables an increase in height and number of layers of printed product. The higher shape retention ratio is used to quantify a high shape retention ability, which is a significant parameter for G3DP's good buildability, as stated in Table 2.

Thus, the approaches employed in various researchers' printability assessment of G3DP are indicated in Table 2, which can work as empirical guidelines in achieving desirable printability. But, since these approaches shall only indirectly relate to characterizing the printing ability of G3DP, they may not be sufficient. Furthermore, no standardized testing methods are available to determine these rheological properties, and research should also focus on this area.

TABLE 1 Testing equipment and procedure for determining rheological parameters of G3DP.

Reference	Testing equipment	Procedure for determining rheological parameters	Shear rate and duration	Rheological model used	Static yield stress	Viscosity	Remark
Guo et al. (2020)	RVDV-2 type rotational viscometer	The viscometer had a default setting for each SR. The mortar's SS was found by measuring the SS 12 times at one SR and averaging the results. Using various rheological models, the parameters associated with the rheological curves and models were employed to calculate YS and PV.	Increased to 40.46 s^{-1} from 6.751 s^{-1} and then back to 6.751 s^{-1}, in 180 s	According to the Bingham model	14.27–106.97 Pa	6.76–8.80 Pa s	The Herschel-Bulkley model outperforms the Bingham model for characterizing fly ash-based 3D printed geopolymer's rheology.
				According to the Herschel-Bulkley model	55.7–103.97 Pa	7.22–8.62 Pa s	
Paul et al. (2018)	Schleibinger Viskomat XL, Rheometer	To perform a flow curve test after loading the material into the container. At rest, the four-blade vane probe requires a higher torque to rotate, and the pick value of the torque is referred to as the static torque. The Viscomat results were converted using Flatt's calibration coefficients to determine PV and SS.	first increasing the speed to 60 rpm for 2 min, then maintaining it at that speed for 2 min, and finally decreasing it by 2 min to zero	Flatt's calibration coefficients	13,522–17401 N/m^2 (DYS = 2,991–3622 N/m^2)	PV = 113–186 N s/m^2	The TX value needs to be more than 10,000 N mm rpm to achieve superior pumpability. The study led to the realization that the V, TX, and YS properties of 3D printable materials have no relationship.
Albar et al. (2020)	KinexusLab + rheometer (Malvern Instruments Ltd., United Kingdom)	AV and SS v/s SR were recorded. The modified-Bingham model (MBM) was chosen as the appropriate model because of the fresh geopolymer mixtures' non-Newtonian character and pseudoplastic behavior.	0.1 s^{-1} and 30 s^{-1} over 22 intervals	Modified-Bingham model (MBM)	25.98–56.29 Pa	8.75–17.06 Pa s	There were no interruptions or collapses in printing a 25-layer, 250 mm-high structure.
Kondepudi and Subramaniam (2021)	AR-G2 strain-controlled rheometer	PV and YS were measured using the cup-and-vane system. YS was determined using constant SR experiments. The hysteresis test determined the mixture's shear response.	ramped up to 40 s^{-1} at a ramp rate of 0.33 s^{-2} in the hysteresis test, and then lowered to zero	Bingham model to match the shear response recorded between 10 and 30 s^{-1}	8.6–1,000 Pa (DYS = 2.86–72 Pa)	0.35–17 Pa s	To ensure the buildability, YS must not drop below 500 Pa. Shape retention seems hindered in the region below 500 Pa YS.
Alghamdi et al. (2019)	Dynamic shear rheometer (TA Instruments AR 2000EX)	During rotational parallel plate rheology, a pre-shear ramp-up phase of roughly 80 s homogenizes the paste, followed by a ramp-up and a ramp-down.	a pre-shear ramp-up phase of roughly 80 s	-	150–700 Pa	-	YS of 700 Pa demonstrated the printability's maximum limit for the investigated mixes.

(Continued on following page)

TABLE 1 (*Continued*) Testing equipment and procedure for determining rheological parameters of G3DP.

Reference	Testing equipment	Procedure for determining rheological parameters	Shear rate and duration	Rheological model used	Static yield stress	Viscosity	Remark
Panda and Tan (2018)	Anton Par MCR 102 rotational rheometer	To determine SS, SYS, and V, vane probe diameters and container geometries were used in conjunction with the measured torque and velocity (in rpm).	Raised from zero to 60 rpm in 1 minute after loading the material into the rheometer, sheared at 60 rpm for 1 minute before returning to zero in a one-time interval	-	0.4–1.0 kPa	-	A freeform structure comprising 60 layers (10 mm layer thickness) of 60 cm height and 35 cm width was printed.
Sun et al. (2020)	Anton Par MCR 301 rotational rheometer	The deceleration phase was chosen to record rheological parameters to counteract the abnormalities during the acceleration phase. Once SS and SR were fit to a curve according to Herschel- Bulkley fluid mode, PV was determined using a least square equation to determine YS.	100 $s^{-1}$was used for 60 s to pre-shear the paste. After 60 s of adjusting from 0.1 s^{-1} to 10 s^{-1}, the increasing SR increased from 10 to 100 s^{-1} for additional 60 s. This was followed by a 60 s decrease in SR, followed by another 60 s decrease in SR.	Herschel-Bulkley fluid model, using the least square equation	0.81–72.25 Pa	5.35–35.09 Pa s	A vase model 200 mm high was printed (shortest diameter = 40 mm, longest diameter = 60 mm).
Ma et al. (2022)	Viskomat NT rheometer with a mortar probe	SR controlled to get PV and DYS. TX was measured by testing SYS at various times.	(i) paste pre-sheared for 60 s at 50 s^{-1} and rested for 120 s; (ii) at a constant speed, paste tested with SR increased to 50 s^{-1} in 1 min from 0 s, maintained at 50 s^{-1} for 1 min; (iii) at a constant speed, SR decreased to 0 s^{-1} in 1 min from 50 s^{-1}	Bingham model	DYS = 209–1,162 Pa	11.43–28.24 Pa s	Fitting of SS versus SR curves
Kondepudi et al. (2022)	Viskomat XL rheometer with AR-G2 strain-controlled mode	(a) Constant SR test for SYS, (b) Hysteresis loop test for PV; and (c) V recovery test for TX.	Constant angular rotation of 0.6 rpm. Angular velocity increased to 30 rpm in 2 min and decreased in 2 min in the hysteresis loop test.	Bingham model	615–6,000 Pa	16–39 Pa s	-

SS = shear stress; SR = shear rate; YS = yield stress; SYS = static yield stress; DYS = dynamic yield stress; V = viscosity; PV = plastic viscosity; AV = apparent viscosity; TX = thixotropy.

3 Structural assessment and performance of G3DP

Various assessment approaches adopted for evaluating the structural properties of G3DP, like green strength, bond strength, flexural strength, and compressive strength, are presented in Table 3.

Compressive strength: Researchers (Panda et al., 2017a; Panda et al., 2017b; Paul et al., 2018) have performed tests to determine the compressive strength of saw-cut cubic samples in three loading orientations to understand better the anisotropic features of printed parts: longitudinal, perpendicular and lateral. But, the compressive strength of casted and printed specimens is still debated. In certain studies (Nerella and Mechtcherine, 2019), the cast specimens had lower compressive strength than printed specimens, while the trend reversed in other studies (Bong et al., 2021). A variety of factors, including the print ink, the printed object's size and shape, the

10.3389/fmats.2023.1241869

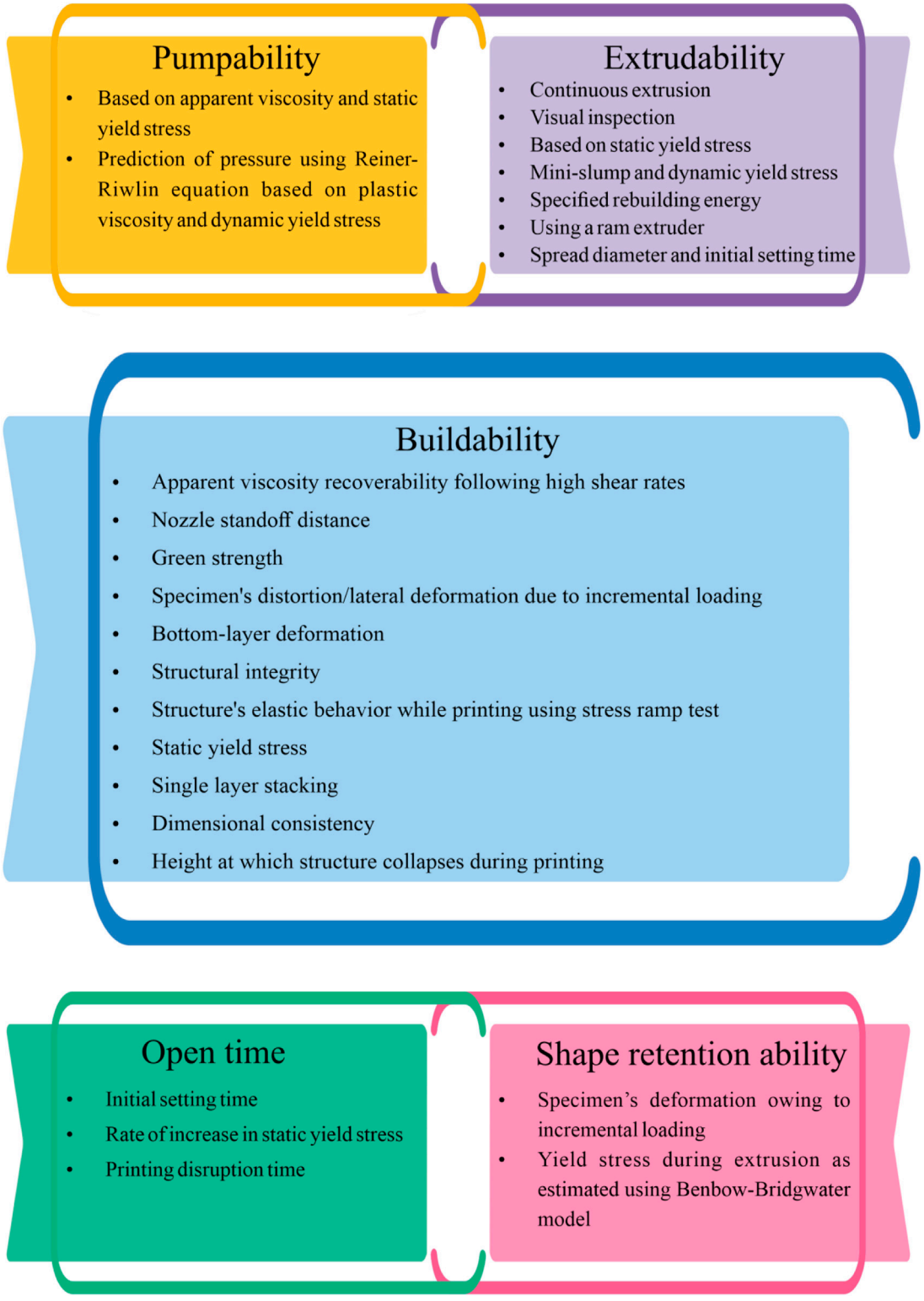

FIGURE 2
Rheology assessment approach for printability characteristics of G3DP.

nozzle's geometry and size, the speed of printing, print time interval, cure conditions, and so on, are implicated in the study's opposite findings. As a result of the factors mentioned above, printing quality and pumping pressure considerably impact the quantity and arrangement of intra- and inter-filament voids, hence the behavior of printed structures. According to the literature, the compressive strength of 3D printed samples is directly influenced by the loading orientation due to anisotropy (Shakor et al., 2021).

TABLE 2 Acceptance criteria for assessing printability characteristics of G3DP.

Reference	Property	Assessment approach	Acceptance criteria (observation and remark)
Muthukrishnan et al. (2021)	Pumpability	Based on AV and SYS	SYS was less than 5 kPa for at least 45 min after mixing, with AV ranging between 10 and 100 Pa s.
Bong et al. (2021)		Reiner-Riwlin equation can be used to predict how much pressure is needed to pressurize G3DP based on measurements of the PV and DYS of the material.	Lower PV and DYS lead to improved pumpability.
Bong et al. (2018), Alghamdi et al. (2019), Panda et al. (2019c), Panda et al. (2020), Bong et al. (2021)	Extrudability	It is evaluated through the continuous extrusion of a single layer for a specific length and visually inspected for shape distortion or discontinuity. The layer width of the printed geopolymer specimen is measured at regular intervals along its length and conformed with the nozzle dimensions.	The extrudability was interpreted and concluded to be satisfactory after the measurements were confirmed.
Ranjbar et al. (2021)		Visual inspection	1. If the layers could not sustain gravity load after printing, the material was classified as too flowable.
			2. If the material had high stiffness, not allowing extrusion or allowing disruptive extrusion, it was classified as not extrudable.
			3. If the material was printable without any discontinuity or defects and retained its geometry, it was classified as printable.
Ranjbar et al. (2021)		Based on SYS	The mix is printable and capable of maintaining its geometrical stability so far as this YS value exceeds the level of stresses present in the printed object.
Panda and Tan (2018)			Geopolymers with SYS between 600 and 1,000 Pa can be expected to extrude smoothly, while those with SYS higher than this range will have difficulty getting enough torque from the rheometers in use, resulting in a low degree of extrusion.
Alghamdi et al. (2019)		Based on the range of mini-slump and DYS	The highest DYS reached 700 Pa from initial mixing, and the highest mini-slump reading. measured < 9 mm. Good extrudability was attained in this range.
Zhang et al. (2018)		Specified rebuilding energy	The greater the specified rebuilding energy, the better the extrudability.
Şahin et al. (2021)		Using a ram extruder	Using the equation $\tau_0 = \sigma_0/\sqrt{3}$, the elongational YS ($\sigma_0$) obtained from the ram extruder is transferred into the shear YS (τ_0) to understand how the activator type/rate used influences the rheological response.
Yuan et al. (2022)		Spread diameter	Extrudability was not achieved for a spread diameter < 200 mm.
Ma et al. (2022)		Spread diameter and initial setting time	Extrudability is acceptable if the spread diameter is > 174 mm and the initial setting time is > 37.5 min.
Panda and Tan (2018), Panda and Tan (2019), Muthukrishnan et al. (2020), Muthukrishnan et al. (2021)	Buildability	AV recoverability following high shear rates	The printing process was mimicked by shearing fresh geopolymers at 0.1 s^{-1} and 100 s^{-1} during a rheological test. The buildability of G3DP was assessed by adjusting the shear rate to 0.1 s^{-1} from 100 s^{-1} and finding that a higher recovery ability led to improved buildability.
Panda and Tan (2018)		Distortion of the printed product subjected to an incremental load of 0.1 N/s	The printed product's distortion was less after the application of load increment.
Panda et al. (2019d)		Monitoring of the nozzle standoff distance of a printed cylinder	Lesser the nozzle standoff distance for the printed cylinder, the better the buildability.
Panda et al. (2019c)		Green strength	High buildability may be hampered by the extruded material's low green strength.

(Continued on following page)

TABLE 2 (*Continued*) Acceptance criteria for assessing printability characteristics of G3DP.

Reference	Property	Assessment approach	Acceptance criteria (observation and remark)
Bong et al. (2019a), Panda and Tan (2019), Panda et al. (2020), Ranjbar et al. (2023)		Bottom-layer deformation of the printed object	Bottom-layer deformation of the printed component was minimum, indicating improved buildability.
Alghamdi et al. (2019), Panda et al. (2019c), Chougan et al. (2020), Bong et al. (2021), Souza et al. (2021)		The structural integrity of the printed product	The printed product should have greater structural integrity and no visible distortion.
Panda et al. (2020), Muthukrishnan et al. (2021), Souza et al. (2021)		Rate of increase in SYS	A higher rate of increase in SYS resulted in superior buildability.
Muthukrishnan et al. (2021)		Elastic behavior of the structure while it is being printed using stress ramp test	The structure exhibited higher elastic modulus while being printed, leading to good buildability.
Muthukrishnan et al. (2021)		The height at which the structure collapses during printing	The greater the height at which the structure collapses during printing, the better the buildability.
Muthukrishnan et al. (2020)		The lateral deformation of the printed structure subjected to vertical loading	The lateral deformation of the printed structure subjected to vertical loading should be minimum.
Ma et al. (2022)		Depending on the height and number of layers of the printed free-wall structure and a square wall structure by single-layer stacking	The greater the height and number of printed layers at which the structure collapses, the better the buildability.
Kondepudi et al. (2022)		To evaluate dimensional consistency based on Print factor along the height, P_Z (i.e., a ratio of the thickness of filament retained post-print to nozzle clearance maintained) and width P_X (i.e., a ratio of nozzle diameter to the width of filament after print)	$P_X \geq 1$ or $P_X \leq 0.63$ are not permissible owing to too high and too low YS. $P_Z \geq 0.75$ represents better buildability.
Yuan et al. (2022)		A load equal to 20 times the specimen's weight is applied on a 50 mm diameter de-molded specimen of mortar mix	The deformation must be less than 0.2% for acceptable buildability.
Chen et al. (2022a)		Slump retention test using 80 mm (height and diameter) cylindrical plastic mold	The compaction of extruded concrete in done manually in the mold, and then it is vertically lifted to record the slump loss under gravity. A 75 mm slump retention was achieved, indicating good buildability.
Panda and Tan (2018)	Open time	Initial setting time	Open time is increased with an increase in the initial setting time.
Panda et al. (2019d), Ranjbar et al. (2021)		Rate of increase in SYS	Open time is increased when the rate of increase in SYS is low.
Ma et al. (2022)		For a constant nozzle geometry, filament height, and print speed, the time at which the printing of a free-wall structure and a square-wall structure by single-layer stacking exhibited disruption	The printing disruption time is considered as open time.
Nematollahi et al. (2018a), Bong et al. (2021), Şahin et al. (2021), Ilcan et al. (2022)	Shape retention ability	Specimen deformation as measured due to pressure of steel plates placed over the specimen	The specimen deformation should be minimum when subjected to incremental loading of steel plates, proving its good shape retention ability. The steel plates were added until the specimen collapsed.
Alghamdi et al. (2019)		YS during extrusion as estimated using the Benbow-Bridgewater model	Better shape retention ability was achieved when the YS exceeded 20 kPa during extrusion.
Bong et al. (2018), Panda and Tan (2018), Bong et al. (2019a), Panda et al. (2019d), Kondepudi et al. (2022)		Shape retention ratio (SRR), i.e., the ratio of the bottom width of the filament extruded to the nozzle opening's width (or height of material retained after lifting the mini-slump cone to the height of the mini-slump cone)	As SRR rises, so does the mixture's capacity to maintain shape.
Kong et al. (2022)		Shape retention ratio (SRR_t) for thickness (SRR_w) for width, i.e., a ratio of specimen thickness/width during measurement and specimen thickness/width when it was just extruded	As SRR_t and SRR_w rise, so does the mixture's capacity to maintain shape.

YS = yield stress; SYS = static yield stress; DYS = dynamic yield stress; V = viscosity; PV = plastic viscosity; AV = apparent viscosity.

TABLE 3 Anisotropy variation and assessment approach for structural characteristics of G3DP.

Reference	Property	Assessment approach	Observation and remark
Panda et al. (2019a), Panda et al. (2019b)	Green strength	Unconfined uniaxial compression tests were carried out on cylindrical samples 140 mm high and 70 mm in diameter.	The variation in behavior is linked to material failure, as older samples exhibit a separate failure plane, whereas younger samples fail via the barreling effect.
Panda et al. (2017a), Paul et al. (2018)	Compressive strength	Loading the printed specimen in lateral, perpendicular, and longitudinal directions	The longitudinal loading orientation had the greatest compressive strength.
Panda et al. (2017b)			In the longitudinal direction, the compressive strength of fiber-reinforced geopolymer dropped relatively. Depending on the capacity of the matrix to handle them, fibers parallel to the loading direction behave as voids.
Demiral et al. (2022)			The perpendicular loading direction had the highest compressive strength.
Pasupathy et al. (2023)			The longitudinal loading direction had the greatest compressive strength, whereas the lateral orientation had the lowest one.
Le et al. (2012b)	Flexural strength	Loading the printed specimen in lateral, perpendicular, and longitudinal directions	The highest tensile stress occurs in the longitudinal direction (i.e., parallel to the extruded filament) at the prism specimen's middle bottom portion, which controls the flexural strength. Improved bottom-layer loading capacity and, as a result, increased flexural capacity in this particular direction is aided by more excellent compaction and a reduced water-to-binder ratio.
Demiral et al. (2022)			The perpendicular loading direction had the highest flexural strength.
Nematollahi et al. (2018a), Bong et al. (2019a), Nematollahi et al. (2019b)	Bond strength	T-sections were attached to the upper and lower surfaces of the two-layered extruded samples using epoxy adhesive.	The horizontal bond among adjacent filaments in the longitudinal direction in the same layer is more potent if the open or delay time is lesser between them.
Demiral et al. (2022)			The bond strength was reduced due to a rise in the viscosity when NaOH molarity and $Ca(OH)_2$ utilization increased from 10 to 12.5 M and beyond 4%, respectively.
Yuan et al. (2022)		Using the slant shear strength test by applying load at a rate of 2.4 kN/s and a 60° inclined angle of the specimen	The interlayer bond strength increased with a rise in sand/binder ratio and a greater silicate modulus but reduced with an increase in fly ash/GGBS ratio in G3DP mixtures.

The G3DP specimens should gain the required compressive strength for construction applications besides satisfying the printability essentials (Bhattacherjee et al., 2021; Izadgoshasb et al., 2021). In an investigation, due to enhanced gel formation, the strength of G3DP and mold-cast samples continuously increased with increasing content of GGBS (Panda et al., 2019c; Chougan et al., 2020). On the contrary, regarding replacing GGBS with silica fume, a steady changing pattern did not prevail for the G3DP's compressive strength, whereas there was a persistent decreasing pattern in the case of mold-cast specimens (Chougan et al., 2020). In some studies, geopolymers were mold-cast to study the effect of additive incorporation on the compressive strength. It was found that poorly dispersed nanoclay particles induced the porosity which caused the compressive strength to reduce by 27.90% with 0.5% nanoclay inclusion in FA-GGBS-based geopolymers (Panda et al., 2019d). The inclusion of sodium carboxymethyl starch and sucrose powder also exhibited a similar influence on the geopolymers' compressive strength (Sun et al., 2020; Bong et al., 2021). In contrast, a 17.8% increase in the compressive strength was observed incorporating 0.1% nano-graphite platelets in FA-GGBS-silica fume-based geopolymer due to crack-bridging mechanism, while further incorporation caused a reduction of the compressive strength (Chougan et al., 2020).

Flexural strength: Researchers also noticed that the G3DP's flexural strength decreased, whereas the mold-cast geopolymers' flexural strength grew as GGBS dose increased, which is linked to the poor bond between layers and material's inferior microstructure (Chougan et al., 2020). With a change in silica fume dosage, the mold-cast and G3DP samples exhibited similar varying patterns of the flexural strength (Chougan et al., 2020).

When sodium carboxymethyl starch was introduced into mold-casted geopolymer, the flexural strength trended downward at various curing ages, with a more pronounced decline at 28 days (Sun et al., 2020). The flexural strength of geopolymers increased by 47.1% after inserting 1.0% nano-graphite platelet because it can successfully block and bridge fractures upon loading (Chougan et al., 2020). According to Chougan et al. (2020), the weak bond state between layers was why the flexural strength of most of the examined G3DP mixes was lower than that of mold-cast geopolymers. For instance, a mold-cast geopolymer containing 5% silica fume had a flexural strength of approximately 38.3% greater than that of G3DP. A conclusion, however, cannot be made solely on these few pertinent studies. Similar to the compressive strength, the G3DP's flexural strength displays anisotropic behavior. If the highest bending stress is created at the bulk material rather than the interface, a printed element's

flexural strength may even be higher than that of a specimen made in a mold (Mohan et al., 2021a).

A study in which a combination of hollow brick, red clay brick, roof tile, concrete waste, and glass waste was used to examine the behavior of construction and demolition waste-based G3DP, the maximum anisotropy variation in the compressive strength values of printed samples subjected to loading in various orientations reached 20%, whereas it was 30% in the flexural strength findings (Demiral et al., 2022). Due to the pores getting filled with the reaction products developed by the extended curing periods of G3DP, the mechanical anisotropy reduces (Chen et al., 2022a). Due to its higher thixotropy and poor activation reactivity, a rise in FA dosage lead to enhanced mechanical anisotropy as a result of high pore content, worsened pore structure between printed layers, and lower mechanical strengths in a study on GGBS-FA-based G3DP (Chen et al., 2022a).

When the printing materials are extruded, the most pressure is applied in a longitudinal direction (Nematollahi et al., 2019b); this is owing to the lack of formwork; the printing materials experience a medium degree of pressure in a perpendicular orientation, notwithstanding the burden of layers (Sanjayan et al., 2018). As a result, there is weakness in the lateral direction. Loading longitudinally facilitates stress transfer, but loading perpendicularly or laterally results in an interfacial slide between filaments (Panda et al., 2017a). In the printed components' lateral, perpendicular, and longitudinal orientations, respectively, low, medium, and high degrees of compaction are exhibited, leading to relatively more voids in the lateral and perpendicular orientations. This problem may be dealt with by providing side trowels at the nozzle orifice to achieve better compaction of the extruded layer.

Green strength and interlayer bond strength: According to a study of the impact of print configuration on structural behavior, geopolymer composites influenced the shear strength more than implanted wire reinforcements in printed specimens (Li et al., 2020). The samples were printed in a concentric pattern and two crosshatch zigzag patterns (90° rotated to each other). The printed specimens of just-add-water geopolymer had the compressive strengths of 10% and 27% lower than the cast one (61.2 MPa) (Bong et al., 2021). Compressive green strength was employed in a study (Panda et al., 2019b) to demonstrate material rebuilding or hardening rate due to flocculation and reactivity (poly-condensation). The early age strength development in conventional liquid-based geopolymers is due to quick reaction product generation. In contrast, it is due to thixotropy and geopolymer reaction combination in one-part geopolymers. The primary distinction between thixotropy and rigidification is that thixotropy is rapidly broken down by shearing action while rigidification is permanent. Another research (Muthukrishnan et al., 2020) aimed to examine microwave heating to modulate the stiffening rate of G3DP to successfully improve the interlayer bond and buildability.

A method of 3D printing called fused deposition modelling (FDM) uses melting thermoplastic filament and layer-by-layer extrusion to produce 3D objects. FDM is frequently used to print small parts, models, and prototypes. Stereolithography (SLA) is a method of 3D printing that builds 3D objects by curing a liquid resin with a UV laser. SLA is frequently used to print intricate, high-resolution items. Selective laser sintering (SLS) is a method of 3D printing that involves layer-by-layer sintering (or fusing) of powdered materials, such as metal, plastic, or ceramic. SLS is frequently used to manufacture practical components with complicated geometry. Binder jetting is a method of 3D printing that involves layer-by-layer selective bond of powdered materials, such as metal, plastic, or ceramic, using a liquid binder. Binder jetting is frequently used to print big, low-resolution pieces.

Thus, the extrusion-based manufacturing process of G3DP could significantly influence its mechanical strength, which is not the case for mold-cast specimens. The mechanical strength of G3DP specimens can be either lesser or more remarkable than the mold-cast geopolymers, depending on the additive manufacturing process and induced interlayer porosity. Further, anomalies regarding the mechanical behavior of G3DP prevail due to various factors, as discussed, which makes its prediction very difficult. Moreover, the anisotropic nature of the layered structure of G3DP evolves as a significant hurdle in applying this innovative technique for field purposes. Extensive investigations are needed to gain a fuller understanding of the structural characteristics of G3DP and discover practical solutions to cater to its anisotropic behavior.

4 Influence of printing process parameters on properties of G3DP

This section reviews the impact of printing process parameters on the rheological and structural properties of G3DP. The 3D printing process parameters, i.e., nozzle design, print time interval, printing speed, printed layer geometry, and printer type, are summarized in Table 4 to understand their influence on the properties of G3DP. It can be observed that rectangular, circular, square, and 45° inclined nozzles are employed for G3DP. The diameter of a circular nozzle ranges from 1.65 to 20 mm, whereas a 30 × 15 mm sized rectangular nozzle is frequently used. Print time interval varies from 0min to 6h, while printing speed varies from 3 to 150 mm/s. The printed layer's length, height, and width range is 50–500 mm, 2.5–40 mm, and 13–300 mm, respectively, as observed in Table 4. A mix that is successfully printable from a particular printer may not necessarily be printable from some other printer, depending on the mixture properties and printer specifications. Printers employed for G3DP are also listed in Table 4.

4.1 Nozzle design

The size and shape of the nozzle have a substantial influence on molding the material's output and defining the buildability of the end product to make a successful print. The nozzle shape and size can be changed according to the object's dimensions and resolution requirements. The circular nozzle causes many voids/holes in the printed product, which may reduce its strength; however, this problem may not be as severe in the case of rectangular or square nozzles (Paul et al., 2018). The circular nozzle is ideal for printing complicated items since it can retain a symmetrical section at various rotational angles. While this may be difficult to do with other types of nozzles, a square nozzle location slips beyond the printing track, whereas a circular nozzle retains the correct positioning. Shakor et al. (2019a) revealed that employing a

TABLE 4 Influence of 3D printing process parameters on performance of G3DP.

Reference	Nozzle design	Print time interval	Printing speed	Layer length (mm)	Layer height (mm)	Layer width (mm)	Type of used printer	Highlight
Li et al. (2020)	15 mm diameter	30 min	60 mm/s	500	6	13	-	To improve the mechanical properties of G3DP, continuous and simultaneous micro-cable strengthening techniques were adopted. But the simultaneous intrusion of reinforcing steel micro-cables with geopolymer extrusion was hindered due to the swaying of the micro-cables. One concentric tube was built and slanted into the nozzle to prevent the swaying of micro-cables during the extrusion process, and a continuous cable was fed from the concentric tube.
Paul et al. (2018)	Rectangular (10 mm × 20 mm), circular (8 mm diameter)	30, 60 min	150 mm/s	500	-	150	Robotic printer	Specimens printed with a rectangular nozzle orifice showed a strength development trend nearly identical to the control samples, but samples printed with a circular nozzle showed a wide range of strength growth. Ultimate compressive strengths were obtained between 36 MPa and 57 MPa.
Albar et al. (2020)	20 mm diameter	10–35 min	20 mm/s	180	10	80	Cementitious-based material rheology served as the basis for the design of the hopper and the extrusion system	Appropriate buildability was achieved by performing a buildability test through the extrusion-based 3D printing of a cylindrical object 250 mm high in 25 layers. The optimum mix exhibited an open time of 20 min, setting time of 33 min, and compressive and flexural strengths of 43.8 MPa and 8.1 MPa, respectively.
Souza et al. (2021)	2 mm aperture	-	3 to 5 mm/s	-	-	-	DuraPrinter E01	Adding a heating element to the printer can speed up the process of geopolymerization and improve paste buildability just before printing.
Ma et al. (2019)	-	-	35 mm/s	400	-	100	-	To satisfy the requirement of reinforced composite consistency, the geopolymer mix's printing rate and the micro-cable's entraining pace must be tuned and matched. The horizontal printing speed was used to establish the micro-cable entraining pace. A maximum of 8 layers were printed.
Panda et al. (2018a)	30 × 15 mm and 20 × 20 mm	1, 5, 10, 15, 20, 35 min, 3 h, 6 h	70, 90, 110 mm/s	350	15	30	4-axis gantry system	Nozzle standoff distance = 0, 2, 4 cm. Average compressive strength was 36 MPa, average tensile strength (dumbbell shape specimens with cross-section 30 mm × 45 mm and gauge length 160 mm) was 1.63 MPa, and 3-point average bending strength was 5.05 MPa, after ambient curing for 28 days.
Al-Qutaifi et al. (2018)	-	5, 10, 15 min	-	160	40	13.33	-	Reducing print time intervals creates strong adhesion between additive layers and improved the flexural strength. Additive layers can be thickened to increase the flexural strength. A maximum of 18 layers were printed. The highest flexural strength measured was 5.46 MPa.
				160	13.33	40		
Panda et al. (2017a)	15 mm × 7 mm	5, 10, 15, 20 min	120 mm/s	500	-	300	6-axis Denso robot	As the print time gap increased, the bond strength decreased.
Panda et al. (2018b)	10 mm diameter	1, 5, 10, 20 min	80 mm/s	400	-	60	4-axis gantry system	The thixotropic property improved as the resting time increased. The compressive strength of the printed specimen was 18.4 MPa.

(Continued on following page)

TABLE 4 (*Continued*) Influence of 3D printing process parameters on performance of G3DP.

Reference	Nozzle design	Print time interval	Printing speed	Layer length (mm)	Layer height (mm)	Layer width (mm)	Type of used printer	Highlight
Kashani and Ngo (2018)	1.65 mm diameter	0, 15, 30, 45 min	25 mm/s	50	2.5 ± 0.2 mm	50	3D-Bioplotter inkjet printer from EnvisionTEC	A maximum of 12 layers were printed. At 21 days, the compressive strength was 50 MPa.
Archez et al. (2021)	10 mm diameter	-	-	-	66% of nozzle diameter		3D printer Potterbot 7	The printed material's flexural strength was measured as 15 MPa.
Nematollahi et al. (2018b)	45° with a 30 mm × 15 mm opening	2 min and 15 min	-	200	15	30	Small-scale custom-made 3D printer	Specimens contain two printed layer filaments. Samples printed with a 2-min delay period had the interlayer strength (0.8–1.3 MPa) that was 63% higher than samples produced with a 15-min delay time, while the compressive strength (19.9–35 MPa, depending on testing direction) was not significantly affected by the delay time. The mean flexural strength with a delay time of 2 min was 6–15% higher than that with a delay time of 15 min.
Nematollahi et al. (2020)	45° with a 30 mm × 15 mm opening	2 min and 15 min	-	200	15	30	Custom-made small-scale 3D printer	Specimens contain two printed layer filaments. Average spread diameters imply a zero-slump mix which is favorable for extrusion. The fresh mixture's open time was nearly 20 min, substantially less than the initial setting time of 65 min. The fresh geopolymer's observed static yield stress was always more significant than the estimated stress caused by the printed layers, regardless of delay duration. Based on the curing temperature, duration, and delay time, the specimens had the compressive strengths ranging from 17.7 to 43.2 MPa, flexural strengths ranging from 2.8 to 6.2 MPa, and inter-layer bond strengths ranging from 0.7 to 2.0 MPa. Depending on the curing circumstances, there was a 25–86% increase in the interlayer bond strength when specimens were extruded with a 2-min delay period rather than a 15-min delay time. The flexural and compressive strengths were not affected by the examined delay intervals.
Bong et al. (2019b)	45° with a 30 mm × 15 mm opening	2 min	35 mm/s	350	15	30	Small-scale custom-made 3D printer	Two types of specimens consisting of only one printed layer and two printed layers were considered for the study. Based on the number of layers printed and loading orientation, the 3D printed samples had compressive strengths ranging from 25.1 to 49.8 MPa, rupture modulus ranging from 8.6 to 10.2 MPa, and deflection capacities ranging from 2.9 to 5.3 mm. The compressive strength of G3DP revealed anisotropic behavior based on the loading orientation, regardless of the quantity of the layers printed. The four-point bending test was employed to evaluate the flexural behavior of G3DP samples, and it was reported to be influenced by the number of layers printed. The specimens with two printed layers had higher first crack strength and rupture modulus than those with only one layer. On the other hand, specimens consisting of only one printed layer have a much

(Continued on following page)

TABLE 4 (*Continued*) Influence of 3D printing process parameters on performance of G3DP.

Reference	Nozzle design	Print time interval	Printing speed	Layer length (mm)	Layer height (mm)	Layer width (mm)	Type of used printer	Highlight
								larger deflection capacity than two printed layer specimens.
Ranjbar et al. (2021)	20 mm × 4 mm	2 min	300 mm/min	90	3.5	-	Desktop HYREL 3D Printer, Engine SR (Standard Resolution) model	If the activator content in a mixture is higher, the printing window gets prolonged. The printing window is dependent on the time and composition of the mix.
Panda et al. (2020)	30 mm × 15 mm	-	60–100 mm/s	-	-	30	4-axis gantry printer	A cylinder having a 20 cm diameter was printed up to 15 layers. Also, a slender twisted column was printed successfully.
Agnoli et al. (2019)	2.25 mm diameter	-	20 mm/s	-	0.6	-	FDM 3D printer, 3Drag, Futura Elettronica, Italy	Printing of 28 mm high hollow cylindrical object (internal diameter 10.5 mm, external diameter 15 mm)
	4 mm diameter		85 mm/s		2		Delta WASP 40100, WASP, Italy	A hollow, self-supporting, non-continuous section structure (height: 45 cm, width: 25.7 cm, depth: 25.7 cm) with a complex geometry was printed successfully.
Ilcan et al. (2022)	20 mm × 20 mm	-	60 mm/s		20		Lab-scale 3D printer	The ratio of the real ultimate height (213.99 mm) of the printed object to the ultimate height (220 mm) measured in the G-code was used to compute the final buildability outcomes (97.3%) of multi-layer specimens (11 layers). The 28-day compressive strength was 36 MPa.
Bong et al. (2022)	20 mm diameter	-	1800 mm/min	400	10	320	Gantry-type 3D concrete printer	A 300 mm square slab comprising five layers with a total length of each layer equal to 4,810 mm was printed without blockages and defects to assess extrudability. A 200 × 300 mm column comprising 23 layers confirmed acceptable buildability.
Muthukrishnan et al. (2022b)	20 mm diameter	-	-	127	-	-	-	2 mixing paddles and a special mixing container with a conical head 30 mm high and having a penetrating needle were built for an in-line high-shear mixer. The mixer was set to three residence times (15–60 s) and three mixing speeds (300, 480, and 750 RPM) to make the new mix. Even though the mix design was kept the same, the Hobart mixer's low mixing energy lowered the beam length by roughly 50% relative to the in-line mixer, enhancing the buildability.
Kondepudi et al. (2022)	30 mm diameter	-	2 cm/s	400	-	-	Gantry-type 3D concrete printer	For dimensional consistency and deformation evaluation, a filament of 400 mm and a rectangular section of 20 mm × 30 mm was printed.
Alghamdi and Neithalath (2019)	Diameter of the barrel, die entry and exit = 35 mm, 10 mm, and 4 mm, respectively	-	20 mm/s	-	3	6	BCN3D Cartesian printer	A cylinder having a total height of 75 mm and 25 layers was printed. The extrusion process, i.e., the extruder geometry, extrusion rate, and pressure, did not significantly affect the pore structure.
Muthukrishnan et al. (2020)	25 mm × 15 mm	1 min	12 mm/s	50	15	25	Lab-scale 3D printer	The bond strength of filaments subjected to microwave heating for 5 seconds and 10 seconds rose by 48.3% and 132% after 7 days and 22.15% and 87.5% percent after 28 days, respectively. At 7 and 28 days, the

(Continued on following page)

TABLE 4 (*Continued*) Influence of 3D printing process parameters on performance of G3DP.

Reference	Nozzle design	Print time interval	Printing speed	Layer length (mm)	Layer height (mm)	Layer width (mm)	Type of used printer	Highlight
								strength decreased by 43% and 29.5%, respectively, if the heating time was longer than 10 s. The printed object's overall moisture loss over 28 days also showed a similar trend. Further, geopolymer mortar subjected to 10 s of microwave heating could recover up to 100% of their initial flow properties, and lateral deformation decreased by 87%. In contrast, those with no thermal treatment could recover only up to 25%. For the filaments, at 5 s and 10 s of microwave exposure, the elastic modulus increased by 207.81 kPa and 1757.38 kPa, respectively. Until 10 s of exposure to microwave radiations, the moisture loss at the surface was negligible.
Kong et al. (2022)	Six different nozzle geometries	-	-	-	-	-	Self-made printer	Various nozzle geometries (22.56 mm diameter, 16.92 mm diameter, square (20 mm side, 15 mm side), and rectangular (28.28 × 14.14 mm, 21.21 × 10.61 mm)) were attempted to confirm good printability of kenaf fiber and kenaf straw core based geopolymer mortars. The mixes could be smoothly extruded.
Pasupathy et al. (2023)	30 mm diameter		10 mm/s	300	20	30	3-axis gantry printer	A cylinder having a total height of 300 mm and approximately 20 layers were printed, confirming the feasible use of brick waste in G3DP.
Muthukrishnan et al. (2022a)	40 mm × 20 mm	30s	-	-	-	-	Customized printer	After deposition of a simply supported G3DP beam 75 mm long, the set-on-demand mixture demonstrated quick strength gain enhancing the buildability through in-line activation of precursor slurry at the print head.
Chen et al. (2022b)	40 mm diameter	5 min	80 mm/s	-	30	-	3-axis gantry printer	During extrusion, pulling force caused due to nozzle motions adds to the elongation of pores in G3DP.
Chougan et al. (2022)	20 mm diameter	-	15 mm/s	-	8	30	Customized gantry 3D printer	Nozzle stand-off distance = 10 mm. A 45-layer twisted column was printed in nearly 22 min successfully.

caulking gun rather than a progressive cavity pump with a robot produced fiber-reinforced mortar with a greater mechanical strength. Additionally, when utilizing a caulking approach for printing, the effects of various nozzle designs were investigated. Using different concrete combinations and a six-degree-of-freedom industrial robot, Shakor et al. (2017) studied the possibility of 3D printing in construction. They emphasized the significance of precise planning and control, combining techniques like damped least squares and resolved motion rate control to create steady transitions during printing. The study assessed the qualities of concrete mixtures, looking at how well they work in 3D printing using experiments including squeeze-flow and velocity control, thus emphasizing the advantage of mortar in printing due to fewer voids.

Enhancing nozzle designs for concrete 3D printing requires considering shaping components, variable flow control, material qualities, and robotic system integration (McGee et al., 2020). Surface quality can be improved by precisely regulating nozzle orientation and tailoring material rheology for various speeds (McGee et al., 2020). To improve overall print performance, surface finish evaluation is continuously conducted, and flow rate modifications may be automated. Thus, 3D printed specimens' structural characteristics are affected by printing factors such as nozzle orifice geometry and object complexity. There are two steps to determine the ideal size of nozzle essential for extrusion-based G3DP: (i) depending on the nozzle's buildability without deforming or collapsing, and (ii) measuring the width of extrude and print detail capabilities of each nozzle (Albar et al., 2020).

While using coarse aggregates can hinder the extrusion process, G3DP frequently uses fine aggregates like river sand and silica sand, with the greatest sand particle size being determined by the nozzle size and pumping capacity of the pump (Paul et al., 2018). To avoid material blockage at the nozzle outlet, most of experiments on G3DP, according to the available literature, have used sand with a maximum particle size of 2 mm and varied aggregate to binder

ratios ranging from 0.55 to 2.0. For instance, it was witnessed that a considerable increase in the static yield stress occurred when sand was gradually added, bringing the aggregate to binder ratio from 1.1 to 1.9. Even with the additional water, this increase rendered the geopolymer mixtures non-extrudable and resulted in blockage at the outflow (Panda and Tan, 2018).

4.2 Print time interval and printing speed

The print time interval is the amount of time between the point at which the material first comes into contact with water and the point at which it becomes printable, i.e., easily transported by pumping and can continuously extrude through the nozzle. It has to do with how the flowability changes over time (Le et al., 2012a). The open time is distinct from the material setting time. Standoff distance (nozzle height from the top surface of filament) is a printer parameter that affects the specimen's bond strength and surface quality. The standoff distance equals the nozzle's width, allowing seamless filament deposition and preventing the print head and filament from interfering (Bos et al., 2016). The experimental findings (Panda et al., 2018a) show that a higher time interval between layers reduces the strength for the same batch of material. However, the nozzle standoff distance and influence of printing speed are improved at lower levels. Due to a moisture exchange event, the bond strength deteriorates after extended printing time intervals and slow printing speed. As the layer at the bottom dries, it takes greater moisture from the recently placed successive layer while permitting little air to escape. This air remains trapped at the interface, resulting in a weak bond strength in printed specimens. The best printing speed can be found by taking into account the material's freshness and the pump's flow rate. Maintaining a balance between these variables ensures that the bead width stays constant throughout the printing operation. The geopolymer's printing window is smaller than that of OPC because of the increased stiffness growth rate of the former. According to Table 4, the fall in horizontal printing speed from 60 mm/s (Li et al., 2020) to 35 mm/s (Ma et al., 2019) permitted a continual layering operation with reduced cold joints, due to a decrease in the time interval between successive layers. Pumping pressure, printing speed, and nozzle size influence the porosity, shape stability, and layer thickness (Kashani and Ngo, 2018). Slower print rates led to longer gaps between layers and escalated the polycondensation mechanisms prior to placing fresh layers because the rate of slump decreased with print speed (Archez et al., 2021). Compared to the initial setting time, the open time was substantially shorter, according to a comparison between the open time calculated from the printed specimens with varied activator/binder ratio and their initial setting time (Ranjbar et al., 2021). Keeping the nozzle geometry and flow rate constant, Panda et al. (2020) conducted trials to arrive at a printing speed of 90 mm/s depending on the condition that the extrudate's width is the same as the nozzle width (30 mm) to confirm sufficient extrudability and buildability. The inclusion of Na_2SiO_3 induced fast hardening of less than 30 min, reducing open time for G3DP with 100% construction and demolition waste as a precursor (Ilcan et al., 2022). The printing time increased and then dropped with an increase in steel slag addition, the shortest time being 35 min, and the longest being 95 min at 0% and 20% steel slag content in G3DP. Resident times and mixing speed revealed interdependence on the yield strength growth rates, where to reach the same yield strength development rate, the residence time decreases with increased mixing speed and vice versa (Muthukrishnan et al., 2022b). In a study (Chen et al., 2022b) on the pore structure of G3DP, it was revealed that nozzle motions and higher speed result in pore elongation of the large pores, specifically during the extrusion process that adversely affects the mechanical properties and interlayer bond. Although the printing process has little effect on the pore connectivity and capillary porosity, the pore volume and elongation phenomenon positively correlate (Chen et al., 2022b). Results from tests on the compressive strength after 28 days revealed that the strength of 3D printed concrete decreased as printing speed increased (Pan et al., 2023). It caused a larger volume of voids between filaments, which was made mainly by the narrowing of the filament width brought on by faster printing speeds, resulting in decreased compressive strength. The buildability of the printed concrete can be improved by lengthening the print time interval (Joh et al., 2020). The buildability of printed concrete was found positively impacted by an increased print time interval in a comparison of printed structures with print time intervals ranging from 36 to 300 s. A reasonable printing quality was obtained at a speed of 1.5 m/min, and a total height of 27 cm was realized without appreciable deformation in the lower layers (Meurer and Classen, 2021). The interlayer bond can be severely impacted by increasing print speed and printhead height, which can result in decreased strength (Marchment et al., 2019). Thus, to have a balance between the buildability and interlayer bond strength of the printed structures, the optimal print time interval and printing speed for 3D concrete printing should be carefully chosen.

The impact of printing process parameters on the rheological and structural behavior of G3DP, as discussed comprehensively in section 4, is presented in a nutshell in Table 5. Table 5 shows that a bigger nozzle results in a coarser structure but better buildability than a smaller nozzle. The finer the features of printed objects, the smaller the nozzle must be. Further, a circular nozzle enhances printability compared to a rectangular nozzle. However, in comparison to a rectangular nozzle, using a circular nozzle may result in increased porosity within the printed layers while adversely affecting the mechanical characteristics of the printed product. Table 5 shows that increasing the print time interval and reducing the printing speed enables enhanced shape retention and excellent buildability. In contrast, increased printing speed increases the porosity and adversely affects the flexural and interlayer bond strengths. Figure 3 presents the schematic representation of the influence of printing process parameters on the rheological and structural characteristics of G3DP.

Thus, the fresh and mechanical properties of G3DP can be regulated through thoughtful nozzle design and by making possible alterations at the printhead to enhance these properties. Further, the printing process demands a balance between print time interval and print speed to control the characteristics of G3DP. 3D concrete printing restricts the use of vibrators for the compaction of the mix. Research should be conducted to find innovative compaction arrangements attached to the printhead to reduce the porosity and attain a denser matrix. Moreover, attachments at the nozzle orifice should be designed to enable scratching of the layer surface,

TABLE 5 Influence of printing process parameters on properties of G3DP.

Reference	Printing process parameter	W	T	SR	PQ	BU	P	CS	FS	IBS
Albar et al. (2020)	Nozzle size					↑				
Paul et al. (2018)	Circular nozzle				↑		↑	↓	↓	↓
Paul et al. (2018)	Rectangular/square nozzle				↓		↓	↑	↑	↑
Panda et al. (2018a), Ranjbar et al. (2021), Ilcan et al. (2022)	Print time interval		↑	↑		↑			↓	↓
Panda et al. (2018a), Kashani and Ngo (2018), Panda et al. (2020), Archez et al. (2021), Chen et al. (2022b)	Printing speed	↑		↓		↓	↑			↓

W = workability; T = thixotropy; SR = shape retention; PQ = print quality; BU = buildability; P = porosity; CS = compressive strength; FS = flexural strength; IBS = interlayer bond strength.

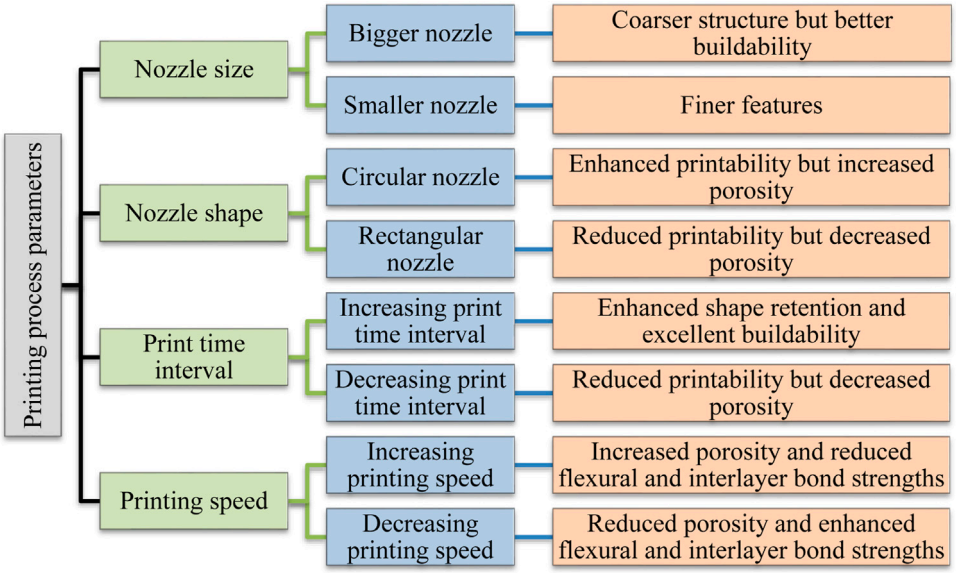

FIGURE 3
Schematic representation of influence of printing process parameters on rheological and structural characteristics of G3DP.

which may provide better bond between successive layers for enhancing the interlayer bond strength.

5 Microstructure of G3DP

To study, examine and understand the microstructure of G3DP, various methods have been adopted, such as scanning electron microscopy (SEM), differential scanning calorimetry (DSC), mercury intrusion porosimetry (MIP), Fourier transform infrared spectroscopy (FT-IR), thermogravimetric analysis (TGA), transmission electron microscopy (TEM), field emission electron microscopy (FESEM), X-ray micro-computed tomography (micro-CT) and Rapid Air techniques, which are discussed in Table 6. SEM and TEM were utilized to assess the morphology of G3DP in terms of the interlayer structural bond, interlayer voids, microcracks, and fracture bridging mechanism in case of additives used such as fibers, structural integrity and matrix quality, which is then linked to the results obtained for the printability and strength properties of G3DP (Table 6). FESEM was adopted to characterize the virgin ingredients and reaction products to realize their impact on the buildability and mechanical behavior of G3DP. Since the extrusion technique for manufacturing G3DP induces the porosity within the layers and layer interface, MIP and micro-CT were used, as given in Table 6, to determine the porosity and analyze the pore structure of G3DP. They were also linked to the print time interval and direction of printing. FT-IR technique is adopted to determine the reactivity and reaction kinetics of ingredients and to study the structure's chemistry variations over time. Thermal analysis plays a significant role in supporting the G3DP's printability and mechanical behavior. TGA and DSC were used to determine the heat flow and cumulative heat released/absorbed, mass loss on thermal treatment, and the strength increment due to exothermic polymerization.

Thus, several researchers have employed the above sophisticated techniques to analyze the microstructure of G3DP. It is understood from Table 6 that the results obtained from applying these methods aid the researchers in correlating and justifying their findings related to the printability and strength characteristics of G3DP. There are in

TABLE 6 Influence of printing process parameters and geopolymer material composition on properties of G3DP.

Reference	Technique adopted (microstructure)	Major finding
Guo et al. (2020)	SEM to assess the morphology of G3DP	In contrast to the dense micro voids and improved geopolymer gel formation in the printed layer's middle portion, many macro voids and a considerable amount of unreacted particles of fly ash and cracks appeared at the surface interlaminar between the extruded layers, implying that the weak zone of the structural characteristics of G3DP sample is located amidst the layers.
		The two interfaces are separated by a long, narrow crack without any intimate connection. Bridges join the two interfaces to develop the strength.
Chougan et al. (2020)		It was determined that when micro-cracks collide with nanographite particles with a greater elastic modulus, additional energy is required to transcend the nanographite particles' high energy absorption, boosting the flexural strength due to crack bridging and fracture blockage.
Geng et al. (2020), Archez et al. (2021)		The interface between the layers is practically undetectable for a brief time duration, giving a material mix that induces high layer adhesion.
		For a lengthy time period, however, a porous interface between the layers is evident.
Pasupathy et al. (2023)		Fragmented morphology, less dense, and more unreacted brick waste particles were seen in G3DP using brick waste.
Kong et al. (2022)		It was confirmed that kenaf fiber and kenaf straw core were responsible for the bridging mechanism and skeleton role, respectively, in G3DP, thus enhancing the form stability and mechanical properties.
Ranjbar et al. (2023)	TEM to assess the morphology of G3DP	It was found that the structural integrity and tubular geometry of the halloysite remained as it is after calcination at 800°C, but the morphology changed at 1,000°C.
	Brunauer–Emmett–Teller surface area analysis	The BET significantly reduced for halloysite, either due to the creation of more stable phases with a low surface area or due to sintering, or both of them.
	TGA for the material characterization	The adsorbed water got evaporated as the temperature rose to 120°C causing a significant loss of mass when halloysite was thermally treated.
	micro-CT to study the pore structure of G3DP	The flexural and compressive strengths improved with halloysite behaving as micro-fiber and micro-filler, and meta-halloysite increasing the binder content in G3DP. However, they were lower at early ages than their mold-cast counterparts.
		The geopolymer matrix containing 5% meta halloysite by weight exhibited the porosity together with the formation of its aggregated particles.
Panda et al. (2019d)	FESEM to characterize the virgin ingredients and reaction products	When clay was included in a geopolymer mix, a heterogeneous aluminosilicate-gel-matrix and partially reacted or unreacted fly ash particles were detected. These particles of unreacted fly ash were detached from the geopolymer matrix, indicating that their adherence to the surrounding gel was weak.
		Several microcracks occurred on the surface of unreacted/partially reacted fly ash grains, possibly linked to the sample's reduced the compressive strength.
Panda et al. (2019c)		One-part geopolymer utilized for 3D printing was found to have an amorphous reaction (potassium aluminosilicate (K-A-S-H) gel) product, as well as unreacted (fly ash and GGBS particles) glassy content, which had a direct impact on its mechanical performance.
		The occurrence of zeolites implicated in the glassy content of the geopolymer material may be credited with the early hardening of the geopolymer material, which results in superior structural build-up.

(Continued on following page)

TABLE 6 (*Continued*) Influence of printing process parameters and geopolymer material composition on properties of G3DP.

Reference	Technique adopted (microstructure)	Major finding
Chougan et al. (2021)	micro-CT and Rapid Air to study the pore structure of G3DP	Some specimens have noticeable porosity anisotropy throughout the height, and in general, the bottom and central sections of specimens include more voids, but careful mixture design helps overcome this barrier.
		As the duration among horizontal layers grew, experts detected an increase in the interlayer porosity.
Ranjbar et al. (2021)	micro-CT	The specimens had badly shaped forms and were challenging to extrude once the open time had surpassed, and many flaws (macro-porosity, de-layering, and shark-skin effects) were found inside the non-extrudable specimens.
Chen et al. (2022b)		Compared to casted geopolymer, G3DP specimens exhibit greater porosity and a coarser dispersion of pore sizes (tiny pores < 400 nm and large voids > 0.2 mm resulting in greater specific surface area > 0.4 mm^3).
Agnoli et al. (2019)	MIP to determine porosity	Biomass addition reduced ambient-cured samples' overall porosity from 68.5% to 46%. It reduced air holes (pores larger than 5,000 nm), encouraging macro pores and mesopores in geopolymer materials.
Chen et al. (2022b)		It was found that G3DP has more elongated pores than spherical pores, oriented along the direction of printing.
Ma et al. (2022)	micro-CT, SEM, Isothermal calorimetry to detect heat generated/absorbed, FT-IR to study the changes in chemical structure over time	OH^- produced by the hydration of steel slag boosted the reaction system's alkalinity and expedited the dissolution of SiO_4^{4-} and AlO_4^{5-}, but its poor reactivity prevents subsequent polymerization.
		The 3D-printed samples had less porosity variation between inter-stripe and intra-stripe positions, decreased pore volume, and no mechanical anisotropy because of the extrusion process and the interlocking of the morphological complementing products together with the main reaction products of CH, AFt, C–S–H, and N(C)-A-S-H gel, as produced from the synergy of quaternary system, which steadily formed to deliver early and later age strength of G3DP.
Muthukrishnan et al. (2021)	DSC to detect heat generated/absorbed, FT-IR	Sucrose powder was employed as a retarder in solid form.
		The solid activator could only be dissolved entirely after 15 min of mixing.
		The cumulative release of heat owing to the polymerization reaction in one-part geopolymer mixtures was linked to the yield strength development through time.
		The delay in the synthesis of C–S–H bridges was primarily accountable for the difference in the rate of the yield strength development of geopolymer with and without sucrose.
		FT-IR spectra revealed ample open time of geopolymer mixtures. Entrapped water molecules from polycondensation reactions are likely released during shearing, lubricating the concrete layers to restore their original rheology.

fact additional advanced techniques that can offer insightful analysis of G3DP. For instance, to better understand the geopolymerization process, crystalline phases inside the printed structures could be identified using X-ray diffraction analysis. The molecular interactions and chemical bond in G3DP can also be studied using nuclear magnetic resonance spectroscopy. In addition, to supplement our macroscopic mechanical testing, nanoindentation testing can be utilized to evaluate the mechanical properties at the nanoscale.

Table 7 compares the density of G3DP with mold-cast geopolymers and presents the porosity of G3DP specimens reported in the literature. From a microstructural standpoint, along with the interlayer porosity (Chougan et al., 2021), at the interface of the reinforcement-geopolymer matrix, G3DP has a problem with voids and connected porosity (Lim et al., 2018). During the printing process, in the case of G3DP mixes having a shorter setting time due to the incorporation of additives, there will be greater porosity and weaker bond between the extruded layers, consequently resulting in lower density of G3DP specimens compared to mold-cast counterparts (Chougan et al., 2020). In the layer-by-layer printing operation, it was reported that there is an unavoidable intrusion of air spaces leading to lower density and higher porosity of about 47.6% compared to mold-cast geopolymers (Bong et al., 2021). Studying the porosity of G3DP in various layers revealed that the bottom layer had a 1.5–9.73% higher porosity than the top layer (Alghamdi et al., 2019). The probable bleeding problem and uneven pressure during extrusion, which elevated the level of

TABLE 7 Density and porosity of G3DP specimens.

Reference	Density (kg/m^3)		Porosity	Remark
	G3DP	Mold-cast geopolymer	G3DP	
Panda et al. (2017a)	2,250	2,150	NR	The weight gain as the layer printing progresses enables the decrease in the porosity near the horizontal interface relative to the vertical interface of layers, resulting in a higher density of G3DP.
Panda et al. (2018a)	2050	1900	NR	
Albar et al. (2020)	2060	2,120	NR	For higher GGBS content, G3DP had lower densities than mold-cast specimens; however, as GGBS content was reduced, the findings were reversed.
Chougan et al. (2020)	2041–2,275	2064.6–2,121.8	NR	The density of G3DP was around 2.68–2.87% less than that of mold-cast specimens when the printed mixtures had a reduced setting time and flowability and for 5% and 10% of silica fume levels.
Sun et al. (2020)	NR	NR	3.98–15.38%	Air voids content rises with increased starch content resulting in greater porosity.
Chougan et al. (2021)	NR	NR	3.34–3.62%	-
Nematollahi et al. (2018a)	NR	NR	10.1–14.1%	High porosity is attributed to the inclusion of fibers, which enhance entrapped air.
Agnoli et al. (2019)	NR	NR	29.5–51.3%	The inclusion of biomass and the high-temperature sintering process controls the porosity. Mercury intrusion porosimetry was used to study the porosity.
Bong et al. (2019b)	1,500	NR	28%	Short polymeric fibers have been added, which has caused an increase in the trapped air in the composite, resulting in this enhanced porosity. The sizeable apparent porosity of G3DP accounts for the low bulk density.
Bong et al. (2021)	2,133	2,156	21.4 ± 0.9%	Mold-cast geopolymer porosity = 14.5 ± 0.9%
Alghamdi and Neithalath (2019)	630–1,150	640–1,160	55–75%	A foaming agent was used to obtain good thermal insulation properties through increased porosity. The thermal conductivities were in the range of 0.15–0.25 W/m-K.

NR = not reported.

inhomogeneity within the printed samples, can be credited for this. This significant variety in the porosity within the samples could result in anisotropy or change in structural characteristics across various load orientations. The density of G3DP was observed to be 4.6–7.89% greater than that of its mold-cast counterparts, irrespective of the kind of binder, which has been related to the increased pressure applied to the specimens during the process of extrusion (Panda et al., 2017a; Panda et al., 2018a).

Thus, it can be concluded that, owing to the difference in manufacturing technique and depending on fresh state properties of G3DP, there is a noticeable difference between the density and porosity characteristics of G3DP specimens and mold-cast geopolymers. It is essential to comprehend the impacts of different printing variables, such as print time interval and printing speed, on the porosity of G3DP to prevent extrusion-induced enhanced porosity.

6 Conclusions

This article highlights the testing equipment and processes adopted and assessment techniques developed for measuring the rheological properties of G3DP. The structural assessment and performance of G3DP are discussed. The effect of parameters related to 3D printing technology adopted for geopolymer, i.e., print interval, print speed, and nozzle design, which play a crucial role in deciding the quality of printed structure, are critically examined. The microstructure of G3DP is also reviewed and discussed in detail. Thus, this article provides a new insight into the area of G3DP.

Based on the presented work, several conclusions can be drawn regarding the rheological assessment, printability evaluation, and microstructural analysis of G3DP materials.

Rheological assessment:

- Rheological properties, including the viscosity and yield stress, are crucial for determining the printability characteristics of G3DP materials.
- Plastic viscosity reflects the cohesiveness and shear-thickening behavior of the fresh mixture, while the yield stress represents the ability to overcome frictional forces and initiate flow.
- Various testing equipment and procedures, such as rotational viscometers and rheometers with different shear rates and durations, are employed to measure rheological parameters.
- The choice of rheological model (e.g., Bingham or Herschel-Bulkley) depends on the material and research objectives.

Printability evaluation:

- The printability characteristics of G3DP are assessed through various approaches, including pumpability, extrudability, buildability, open time, and shape retention ability.
- Assessment criteria include apparent viscosity, static yield stress, structural integrity, slump, spread diameter, green strength, and dimensional consistency.

- Specific rheological and mechanical properties influence printability evaluation, requiring standardized testing methods for accurate and reliable results.

Microstructural analysis:

- Advanced techniques such as SEM, TEM, DSC, MIP, FT-IR, TGA, micro-CT, FESEM, and Rapid Air are employed to analyze the microstructure of G3DP.
- SEM and TEM observations reveal essential information about the morphology, structural bond, voids, cracks, and fracture-bridging mechanisms of G3DP.
- MIP and micro-CT provide insights into the porosity and pore structure of G3DP, primarily related to extrusion-induced porosity within the layers and layer interface.
- FT-IR and thermal analysis techniques offer valuable data on reactivity, reaction kinetics, chemistry variations, and heat flow during printing.
- G3DP specimens generally exhibit lower density and higher porosity compared to mold-cast geopolymers due to extrusion-induced porosity and the intrusion of air spaces during layer-by-layer printing.

General Conclusions:

- Optimal rheological properties, including lower viscosity and appropriate yield stress, are essential for achieving good pumpability, extrudability, buildability, and shape retention in G3DP.
- Nozzle design, print time interval, and printing speed significantly influence the structural characteristics and printability of G3DP.
- The anisotropic behavior and interlayer porosity present challenges in achieving consistent mechanical strength and structural integrity in G3DP.
- Further research is needed to develop strategies that enhance the interlayer bond, minimize porosity, and address anisotropic effects in G3DP.
- Standardized testing methods and comprehensive analysis techniques are essential for accurately evaluating and comparing G3DP materials.

In conclusion, the presented work highlights the importance of rheological assessment, printability evaluation, and microstructural analysis in understanding and optimizing G3DP materials. It provides valuable insights into the influence of various factors on the printability, mechanical properties, and microstructure of G3DP. The conclusions drawn from this work contribute to developing improved techniques and strategies for enhancing the performance and application of G3DP in the field of 3D concrete printing.

7 Challenges and research opportunities

The comprehensive review conducted in this work has identified several challenges and research opportunities that need to be addressed to advance the geopolymer additive manufacturing field (G3DP). These include:

- Porosity control and self-healing: The extrusion manufacturing process leads to the porosity within the layers of the printed product. The incorporation of self-healing agents, such as super absorbent polymers, to control porosity at the layer interface of G3DP should be explored. This can help mitigate shrinkage phenomena and improve the overall structural integrity of printed components.
- Anisotropic behavior: An inherent characteristic of 3D printed components is their anisotropic nature. To address this, modern techniques like carbon/glass fiber wrapping and geosynthetics should be explored to control and manipulate the anisotropic behavior of G3DP structures.
- Durability and microstructure: Long-term performance prediction of G3DP requires extensive research on its durability. Understanding the reaction mechanisms and thoroughly examining the microstructure of G3DP is crucial for comprehending its behavior over time.
- Lateral load-carrying capacity and impact resistance: Research is needed to investigate the lateral load-carrying capacity and impact resistance of G3DP components. This will help determine their suitability for structural applications and ensure their safety and reliability.
- Sustainability and life cycle assessment: The sustainability aspects and life cycle assessment of G3DP need to be studied to evaluate its environmental impact and resource efficiency. This research will contribute to the development of more sustainable construction practices.
- Standardized testing methods and non-destructive testing: There is a lack of standardized testing methods to determine the rheological properties of G3DP materials. Further research should focus on developing reliable testing protocols. Additionally, exploring non-destructive testing techniques will help correlate observations with the properties of G3DP and ensure quality control.
- Topological optimization and material usage reduction: Topological optimization strategies should be studied to minimize material usage in G3DP. These strategies can help optimize the internal structures of printed components, reducing material waste and improving resource efficiency.
- Finite element modeling (FEM): Analyzing the structural behavior of G3DP using FEM can provide insights into its mechanical performance and aid in the design optimization process.
- Controlling mix design and process parameters: It is essential to develop methods for controlling the mix design, rheological properties, and structural properties of G3DP materials before printing. This includes the ability to forecast and regulate print process parameters and composition parameters. Machine learning and numerical modeling techniques can be employed to achieve these goals, facilitating the broader adoption of 3D printing in the construction industry.

These challenges and research opportunities outlined in the work contribute to the future trends in the additive manufacturing of geopolymer materials. By addressing these issues, researchers and industry professionals can enhance the performance, sustainability, and applicability of G3DP, paving the way for its widespread adoption in various construction applications.

Author contributions

Conceptualization, PB, AB, and SS; methodology, PB, AB, and SS; validation, AB and SS; formal analysis, AB; investigation, PB, AB, and SS; resources, AB; writing—original draft preparation, PB, AB, and SS; writing—review and editing, AB. All authors contributed to the article and approved the submitted version.

Conflict of interest

The authors declare that the research was conducted in the absence of any commercial or financial relationships that could be construed as a potential conflict of interest.

Publisher's note

All claims expressed in this article are solely those of the authors and do not necessarily represent those of their affiliated organizations, or those of the publisher, the editors and the reviewers. Any product that may be evaluated in this article, or claim that may be made by its manufacturer, is not guaranteed or endorsed by the publisher.

References

Agnoli, E., Ciapponi, R., Levi, M., and Turri, S. (2019). Additive manufacturing of geopolymers modified with microalgal biomass biofiller from wastewater treatment plants. *Materials* 12, 1004. doi:10.3390/ma12071004

Albar, A., Chougan, M., Al-Kheetan, M. J., Swash, M. R., and Ghaffar, S. H. (2020). Effective extrusion-based 3D printing system design for cementitious-based materials. *Results Eng.* 6, 100135. doi:10.1016/j.rineng.2020.100135

Alghamdi, H., Nair, S. A., and Neithalath, N. (2019). Insights into material design, extrusion rheology, and properties of 3D-printable alkali-activated fly ash-based binders. *Mater. Des.* 167, 107634. doi:10.1016/j.matdes.2019.107634

Alghamdi, H., and Neithalath, N. (2019). Synthesis and characterization of 3D-printable geopolymeric foams for thermally efficient building envelope materials. *Cem. Concr. Compos.* 104, 103377. doi:10.1016/j.cemconcomp.2019.103377

Al-Noaimat, Y. A., Ghaffar, S. H., Chougan, M., and Al-Kheetan, M. J. (2022). A review of 3D printing low-carbon concrete with one-part geopolymer: engineering, environmental and economic feasibility. *Case Stud. Constr. Mater.* 18, e01818. doi:10.1016/j.cscm.2022.e01818

Al-Qutaifi, S., Nazari, A., and Bagheri, A. (2018). Mechanical properties of layered geopolymer structures applicable in concrete 3D-printing. *Constr. Build. Mater.* 176, 690–699. doi:10.1016/j.conbuildmat.2018.04.195

Archez, J., Texier-Mandoki, N., Bourbon, X., Caron, J.-F., and Rossignol, S. (2021). Shaping of geopolymer composites by 3D printing. *J. Build. Eng.* 34, 101894. doi:10.1016/j.jobe.2020.101894

Baduge, S. K., Navaratnam, S., Abu-Zidan, Y., Mccormack, T., Nguyen, K., Mendis, P., et al. (2021). "Improving performance of additive manufactured (3D printed) concrete: a review on material mix design, processing, interlayer bonding, and reinforcing methods," in *Structures* (Netherlands: Elsevier), 1597–1609. doi:10.1016/j.istruc.2020.12.061

Bhattacherjee, S., Basavaraj, A. S., Rahul, A., Santhanam, M., Gettu, R., Panda, B., et al. (2021). Sustainable materials for 3D concrete printing. *Cem. Concr. Compos.* 122, 104156. doi:10.1016/j.cemconcomp.2021.104156

Bingham, E. C. (1922). "Fluidity and plasticity," in *Eugene C. Bingham* (New York: McGraw-Hill Book Company, Inc).

Bong, S. H., Nematollahi, B., Nazari, A., Xia, M., and Sanjayan, J. (2019a). Method of optimisation for ambient temperature cured sustainable geopolymers for 3D printing construction applications. *Materials* 12, 902. doi:10.3390/ma12060902

Bong, S. H., Nematollahi, B., Nazari, A., Xia, M., and Sanjayan, J. G. (2018). "Fresh and hardened properties of 3D printable geopolymer cured in ambient temperature," in *RILEM international conference on concrete and digital fabrication* (Berlin, Germany: Springer), 3–11. doi:10.1007/978-3-319-99519-9_1

Bong, S. H., Nematollahi, B., Xia, M., Ghaffar, S. H., Pan, J., and Dai, J.-G. (2022). Properties of additively manufactured geopolymer incorporating mineral wollastonite microfibers. *Constr. Build. Mater.* 331, 127282. doi:10.1016/j.conbuildmat.2022.127282

Bong, S. H., Nematollahi, B., Xia, M., Nazari, A., Sanjayan, J., and Pan, J. (2019b). "Properties of 3D-printable ductile fibre-reinforced geopolymer composite for digital construction applications," in *Rheology and processing of construction materials* (Berlin, Germany: Springer), 363–372. doi:10.1007/978-3-030-22566-7_42

Bong, S. H., Xia, M., Nematollahi, B., and Shi, C. (2021). Ambient temperature cured 'just-add-water'geopolymer for 3D concrete printing applications. *Cem. Concr. Compos.* 121, 104060. doi:10.1016/j.cemconcomp.2021.104060

Bos, F., Wolfs, R., Ahmed, Z., and Salet, T. (2016). Additive manufacturing of concrete in construction: potentials and challenges of 3D concrete printing. *Virtual Phys. Prototyp.* 11, 209–225. doi:10.1080/17452759.2016.1209867

Buswell, R. A., De Silva, W. L., Jones, S. Z., and Dirrenberger, J. (2018). 3D printing using concrete extrusion: a roadmap for research. *Cem. Concr. Res.* 112, 37–49. doi:10.1016/j.cemconres.2018.05.006

Buswell, R. A., Soar, R. C., Gibb, A. G., and Thorpe, A. (2007). Freeform construction: mega-scale rapid manufacturing for construction. *Automation Constr.* 16, 224–231. doi:10.1016/j.autcon.2006.05.002

Cao, R., Li, B., You, N., Zhang, Y., and Zhang, Z. (2018). Properties of alkali-activated ground granulated blast furnace slag blended with ferronickel slag. *Constr. Build. Mater.* 192, 123–132. doi:10.1016/j.conbuildmat.2018.10.112

Cesaretti, G., Dini, E., De Kestelier, X., Colla, V., and Pambaguian, L. (2014). Building components for an outpost on the Lunar soil by means of a novel 3D printing technology. *Acta Astronaut.* 93, 430–450. doi:10.1016/j.actaastro.2013.07.034

Chen, Y., Jia, L., Liu, C., Zhang, Z., Ma, L., Chen, C., et al. (2022a). Mechanical anisotropy evolution of 3D-printed alkali-activated materials with different GGBFS/FA combinations. *J. Build. Eng.* 50, 104126. doi:10.1016/j.jobe.2022.104126

Chen, Y., Zhang, Y., Xie, Y., Zhang, Z., and Banthia, N. (2022b). Unraveling pore structure alternations in 3D-printed geopolymer concrete and corresponding impacts on macro-properties. *Addit. Manuf.* 59, 103137. doi:10.1016/j.addma.2022.103137

Chougan, M., Ghaffar, S. H., Jahanzat, M., Albar, A., Mujaddedi, N., and Swash, R. (2020). The influence of nano-additives in strengthening mechanical performance of 3D printed multi-binder geopolymer composites. *Constr. Build. Mater.* 250, 118928. doi:10.1016/j.conbuildmat.2020.118928

Chougan, M., Ghaffar, S. H., Nematollahi, B., Sikora, P., Dorn, T., Stephan, D., et al. (2022). Effect of natural and calcined halloysite clay minerals as low-cost additives on the performance of 3D-printed alkali-activated materials. *Mater. Des.* 223, 111183. doi:10.1016/j.matdes.2022.111183

Chougan, M., Ghaffar, S. H., Sikora, P., Chung, S.-Y., Rucinska, T., Stephan, D., et al. (2021). Investigation of additive incorporation on rheological, microstructural and mechanical properties of 3D printable alkali-activated materials. *Mater. Des.* 202, 109574. doi:10.1016/j.matdes.2021.109574

Craveiroa, F., Duartec, J. P., Bartoloa, H., and Bartolod, P. J. (2019). Additive manufacturing as an enabling technology for digital construction: a perspective on Construction 4.0. *Sustain. Dev.* 4, 251–267. doi:10.1016/j.autcon.2019.03.011

Deb, P. S., Nath, P., and Sarker, P. K. (2014). The effects of ground granulated blast-furnace slag blending with fly ash and activator content on the workability and strength properties of geopolymer concrete cured at ambient temperature. *Mater. Des.* 62, 32–39. doi:10.1016/j.matdes.2014.05.001

Demiral, N. C., Ekinci, M. O., Sahin, O., Ilcan, H., Kul, A., Yildirim, G., et al. (2022). Mechanical anisotropy evaluation and bonding properties of 3D-printable construction and demolition waste-based geopolymer mortars. *Cem. Concr. Compos.* 134, 104814. doi:10.1016/j.cemconcomp.2022.104814

De Schutter, G., Lesage, K., Mechtcherine, V., Nerella, V. N., Habert, G., and Agusti-Juan, I. (2018). Vision of 3D printing with concrete—technical, economic and environmental potentials. *Cem. Concr. Res.* 112, 25–36. doi:10.1016/j.cemconres.2018.06.001

Duxson, P., Provis, J. L., Lukey, G. C., and Van Deventer, J. S. (2007). The role of inorganic polymer technology in the development of 'green concrete. *Cem. Concr. Res.* 37, 1590–1597. doi:10.1016/j.cemconres.2007.08.018

Elsayed, H., Gobbin, F., Picicco, M., Italiano, A., and Colombo, P. (2022). Additive manufacturing of inorganic components using a geopolymer and binder jetting. *Addit. Manuf.* 56, 102909. doi:10.1016/j.addma.2022.102909

Fu, S., He, P., Wang, M., Wang, M., Wang, R., Yuan, J., et al. (2019). Monoclinic-celsian ceramics formation: through thermal treatment of ion-exchanged 3D printing geopolymer precursor. *J. Eur. Ceram. Soc.* 39, 563–573. doi:10.1016/j.jeurceramsoc.2018.08.036

Gao, Y., Duan, K., Xiang, S., and Zeng, W. (2021). Basic properties of fly ash/slag-concrete slurry waste geopolymer activated by sodium carbonate and different silicon sources. *Front. Mater.* 8, 751585. doi:10.3389/fmats.2021.751585

Geng, Z., She, W., Zuo, W., Lyu, K., Pan, H., Zhang, Y., et al. (2020). Layer-interface properties in 3D printed concrete: dual hierarchical structure and micromechanical characterization. *Cem. Concr. Res.* 138, 106220. doi:10.1016/j.cemconres.2020.106220

Ghaffar, S. H., Corker, J., and Fan, M. (2018). Additive manufacturing technology and its implementation in construction as an eco-innovative solution. *Automation Constr.* 93, 1–11. doi:10.1016/j.autcon.2018.05.005

Gonçalves, N. P., Olhero, S. M., Labrincha, J. A., and Novais, R. M. (2023). 3D-printed red mud/metakaolin-based geopolymers as water pollutant sorbents of methylene blue. *J. Clean. Prod.* 383, 135315. doi:10.1016/j.jclepro.2022.135315

Gowripalan, N., Shakor, P., and Rocker, P. (2021). Pressure exerted on formwork by self-compacting concrete at early ages: a review. *Case Stud. Constr. Mater.* 15, e00642. doi:10.1016/j.cscm.2021.e00642

Guo, X., Yang, J., and Xiong, G. (2020). Influence of supplementary cementitious materials on rheological properties of 3D printed fly ash based geopolymer. *Cem. Concr. Compos.* 114, 103820. doi:10.1016/j.cemconcomp.2020.103820

Hackley, V. A., and Ferraris, C. F. (2001). *Guide to rheological nomenclature: measurements in ceramic particulate systems*. Berlin, Germany: Springer.

Herschel, W. H. (1924). Consistency of rubber benzene solutions. *Industrial Eng. Chem.* 16, 927. doi:10.1021/ie50177a019

Humad, A. M., Kothari, A., Provis, J. L., and Cwirzen, A. (2019). The effect of blast furnace slag/fly ash ratio on setting, strength, and shrinkage of alkali-activated pastes and concretes. *Front. Mater.* 6, 9. doi:10.3389/fmats.2019.00009

Ilcan, H., Sahin, O., Kul, A., Yildirim, G., and Sahmaran, M. (2022). Rheological properties and compressive strength of construction and demolition waste-based geopolymer mortars for 3D-Printing. *Constr. Build. Mater.* 328, 127114. doi:10.1016/j.conbuildmat.2022.127114

Izadgoshasb, H., Kandiri, A., Shakor, P., Laghi, V., and Gasparini, G. (2021). Predicting compressive strength of 3D printed mortar in structural members using machine learning. *Appl. Sci.* 11, 10826. doi:10.3390/app112210826

Jayathilakage, R., Rajeev, P., and Sanjayan, J. (2022). Rheometry for concrete 3D printing: a review and an experimental comparison. *Buildings* 12, 1190. doi:10.3390/buildings12081190

Joh, C., Lee, J., Bui, T. Q., Park, J., and Yang, I.-H. (2020). Buildability and mechanical properties of 3D printed concrete. *Materials* 13, 4919. doi:10.3390/ma13214919

Kashani, A., and Ngo, T. (2018). "Optimisation of mixture properties for 3D printing of geopolymer concrete," in *Isarc. Proceedings of the international symposium on automation and robotics in construction* (Berlin, Germany: IAARC Publications), 1–8. doi:10.22260/ISARC2018/0037

Khan, M. (2020). Mix suitable for concrete 3D printing: a review. *Mater. Today Proc.* 32, 831–837. doi:10.1016/j.matpr.2020.03.825

Khan, M. S., Sanchez, F., and Zhou, H. (2020). 3-D printing of concrete: beyond horizons. *Cem. Concr. Res.* 133, 106070. doi:10.1016/j.cemconres.2020.106070

Khoshnevis, B. (2004). Automated construction by contour crafting—related robotics and information technologies. *Automation Constr.* 13, 5–19. doi:10.1016/j.autcon.2003.08.012

Khoshnevis, B., Hwang, D., Yao, K.-T., and Yeh, Z. (2006). Mega-scale fabrication by contour crafting. *Int. J. Industrial Syst. Eng.* 1, 301–320. doi:10.1504/IJISE.2006.009791

Kondepudi, K., and Subramaniam, K. V. (2021). Formulation of alkali-activated fly ash-slag binders for 3D concrete printing. *Cem. Concr. Compos.* 119, 103983. doi:10.1016/j.cemconcomp.2021.103983

Kondepudi, K., Subramaniam, K. V., Nematollahi, B., Bong, S. H., and Sanjayan, J. (2022). Study of particle packing and paste rheology in alkali activated mixtures to meet the rheology demands of 3D Concrete Printing. *Cem. Concr. Compos.* 131, 104581. doi:10.1016/j.cemconcomp.2022.104581

Kong, X., Dai, L., Wang, Y., Qiao, D., Hou, S., and Wang, S. (2022). Influence of kenaf stalk on printability and performance of 3D printed industrial tailings based geopolymer. *Constr. Build. Mater.* 315, 125787. doi:10.1016/j.conbuildmat.2021.125787

Korniejenko, K., Kejzlar, P., and Louda, P. (2022a). The influence of the material structure on the mechanical properties of geopolymer composites reinforced with short fibers obtained with additive technologies. *Int. J. Mol. Sci.* 23, 2023. doi:10.3390/ijms23042023

Korniejenko, K., Pławecka, K., and Kozub, B. (2022b). An overview for modern energy-efficient solutions for lunar and martian habitats made based on geopolymers composites and 3D printing technology. *Energies* 15, 9322. doi:10.3390/en15249322

Labonnote, N., Rønnquist, A., Manum, B., and Rüther, P. (2016). Additive construction: state-of-the-art, challenges and opportunities. *Automation Constr.* 72, 347–366. doi:10.1016/j.autcon.2016.08.026

Lao, J.-C., Xu, L.-Y., Huang, B.-T., Zhu, J.-X., Khan, M., and Dai, J.-G. (2023). Utilization of sodium carbonate activator in strain-hardening ultra-high-performance geopolymer concrete (SH-UHPGC). *Front. Mater.* 10, 1–12. doi:10.3389/fmats.2023.1142237

Le, T. T., Austin, S. A., Lim, S., Buswell, R. A., Gibb, A. G., and Thorpe, T. (2012a). Mix design and fresh properties for high-performance printing concrete. *Mater. Struct.* 45, 1221–1232. doi:10.1617/s11527-012-9828-z

Le, T. T., Austin, S. A., Lim, S., Buswell, R. A., Law, R., Gibb, A. G., et al. (2012b). Hardened properties of high-performance printing concrete. *Cem. Concr. Res.* 42, 558–566. doi:10.1016/j.cemconres.2011.12.003

Li, Z., Li, Y., Shi, B., Tang, D., Wang, Y., and Hao, L. (2022). Dual gradient direct ink writing of functional geopolymer-based carbonyl-iron/graphene composites for adjustable broadband microwave absorption. *Ceram. Int.* 48, 9277–9285. doi:10.1016/j.ceramint.2021.12.114

Li, Z., Wang, L., and Ma, G. (2020). Mechanical improvement of continuous steel microcable reinforced geopolymer composites for 3D printing subjected to different loading conditions. *Compos. Part B Eng.* 187, 107796. doi:10.1016/j.compositesb.2020.107796

Lim, J. H., Panda, B., and Pham, Q.-C. (2018). Improving flexural characteristics of 3D printed geopolymer composites with in-process steel cable reinforcement. *Constr. Build. Mater.* 178, 32–41. doi:10.1016/j.conbuildmat.2018.05.010

Lim, S., Buswell, R. A., Le, T. T., Austin, S. A., Gibb, A. G., and Thorpe, T. (2012). Developments in construction-scale additive manufacturing processes. *Automation Constr.* 21, 262–268. doi:10.1016/j.autcon.2011.06.010

Liu, X., Ma, S., He, P., Wang, M., Duan, X., Jia, D., et al. (2023). 3D printing of green and environment-friendly rGO@ ZnO/GP for removal of methylene blue from wastewater. *J. Phys. Chem. Solids* 174, 111158. doi:10.1016/j.jpcs.2022.111158

Luukkonen, T., Abdollahnejad, Z., Yliniemi, J., Kinnunen, P., and Illikainen, M. (2018). One-part alkali-activated materials: a review. *Cem. Concr. Res.* 103, 21–34. doi:10.1016/j.cemconres.2017.10.001

Luukkonen, T., Yliniemi, J., Sreenivasan, H., Ohenoja, K., Finnilä, M., Franchin, G., et al. (2020). Ag-or Cu-modified geopolymer filters for water treatment manufactured by 3D printing, direct foaming, or granulation. *Sci. Rep.* 10, 7233. doi:10.1038/s41598-020-64228-5

Ly, O., Yoris-Nobile, A. I., Sebaibi, N., Blanco-Fernandez, E., Boutouil, M., Castro-Fresno, D., et al. (2021). Optimisation of 3D printed concrete for artificial reefs: biofouling and mechanical analysis. *Constr. Build. Mater.* 272, 121649. doi:10.1016/j.conbuildmat.2020.121649

Ma, G., Li, Z., Wang, L., and Bai, G. (2019). Micro-cable reinforced geopolymer composite for extrusion-based 3D printing. *Mater. Lett.* 235, 144–147. doi:10.1016/j.matlet.2018.09.159

Ma, G., and Wang, L. (2018). A critical review of preparation design and workability measurement of concrete material for largescale 3D printing. *Front. Struct. Civ. Eng.* 12, 382–400. doi:10.1007/s11709-017-0430-x

Ma, G., Yan, Y., Zhang, M., and Sanjayan, J. (2022). Effect of steel slag on 3D concrete printing of geopolymer with quaternary binders. *Ceram. Int.* 48, 26233–26247. doi:10.1016/j.ceramint.2022.05.305

Ma, S., Yang, H., Fu, S., He, P., Duan, X., Yang, Z., et al. (2023). Additive manufacturing of geopolymers with hierarchical porosity for highly efficient removal of Cs+. *J. Hazard. Mater.* 443, 130161. doi:10.1016/j.jhazmat.2022.130161

Ma, S., Yang, H., Zhao, S., He, P., Zhang, Z., Duan, X., et al. (2021). 3D-printing of architectured short carbon fiber-geopolymer composite. *Compos. Part B Eng.* 226, 109348. doi:10.1016/j.compositesb.2021.109348

Marchment, T., Sanjayan, J. G., Nematollahi, B., and Xia, M. (2019). "Interlayer strength of 3D printed concrete: influencing factors and method of enhancing," in *3D concrete printing technology* (Netherlands: Elsevier), 241–264. doi:10.1016/B978-0-12-815481-6.00012-9

Mcgee, W., Ng, T. Y., Yu, K., and Li, V. C. (2020). "Extrusion nozzle shaping for improved 3DP of engineered cementitious composites (ECC/SHCC)," in *Second RILEM international conference on concrete and digital fabrication: digital concrete* (Berlin, Germany: Springer), 916–925. doi:10.1007/978-3-030-49916-7_89

Mechtcherine, V., Nerella, V. N., Will, F., Näther, M., Otto, J., and Krause, M. (2019). Large-scale digital concrete construction–CONPrint3D concept for on-site, monolithic 3D-printing. *Automation Constr.* 107, 102933. doi:10.1016/j.autcon.2019.102933

Meng, T., Yang, X., Yu, Y., Yu, H., and Huang, M. (2021). Hybrid effect of PVA fibre and carbon nanotube on the mechanical properties and microstructure of geopolymers. *Front. Mater.* 513. doi:10.3389/fmats.2021.773103

Meurer, M., and Classen, M. (2021). Mechanical properties of hardened 3D printed concretes and mortars—development of a consistent experimental characterization strategy. *Materials* 14, 752. doi:10.3390/ma14040752

Mohan, M. K., Rahul, A., De Schutter, G., and Van Tittelboom, K. (2021a). Extrusion-based concrete 3D printing from a material perspective: a state-of-the-art review. *Cem. Concr. Compos.* 115, 103855. doi:10.1016/j.cemconcomp.2020.103855

Mohan, M. K., Rahul, A., Van Tittelboom, K., and De Schutter, G. (2021b). Rheological and pumping behaviour of 3D printable cementitious materials with varying aggregate content. *Cem. Concr. Res.* 139, 106258. doi:10.1016/j.cemconres.2020.106258

Muthukrishnan, S., Ramakrishnan, S., and Sanjayan, J. (2020). Effect of microwave heating on interlayer bonding and buildability of geopolymer 3D concrete printing. *Constr. Build. Mater.* 265, 120786. doi:10.1016/j.conbuildmat.2020.120786

Muthukrishnan, S., Ramakrishnan, S., and Sanjayan, J. (2021). Effect of alkali reactions on the rheology of one-part 3D printable geopolymer concrete. *Cem. Concr. Compos.* 116, 103899. doi:10.1016/j.cemconcomp.2020.103899

Muthukrishnan, S., Ramakrishnan, S., and Sanjayan, J. (2022a). In-line activation of geopolymer slurry for concrete 3D printing. *Cem. Concr. Res.* 162, 107008. doi:10.1016/j.cemconres.2022.107008

Muthukrishnan, S., Ramakrishnan, S., and Sanjayan, J. (2022b). Set on demand geopolymer using print head mixing for 3D concrete printing. *Cem. Concr. Compos.* 128, 104451. doi:10.1016/j.cemconcomp.2022.104451

Nagaraju, T. V., Bahrami, A., Azab, M., and Naskar, S. (2023). Development of sustainable high performance geopolymer concrete and mortar using agricultural biomass-A strength performance and sustainability analysis. *Front. Mater.* 10. doi:10.3389/fmats.2023.1128095

Nair, S. A., Panda, S., Santhanam, M., Sant, G., and Neithalath, N. (2020). A critical examination of the influence of material characteristics and extruder geometry on 3D printing of cementitious binders. *Cem. Concr. Compos.* 112, 103671. doi:10.1016/j.cemconcomp.2020.103671

Nematollahi, B., Bong, S. H., Xia, M., and Sanjayan, J. (2020). "Digital fabrication of 'just-add-water'geopolymers: effects of curing condition and print-time interval," in *RILEM international conference on concrete and digital fabrication* (Berlin, Germany: Springer), 93–102. doi:10.1007/978-3-030-49916-7_10

Nematollahi, B., Vijay, P., Sanjayan, J., Nazari, A., Xia, M., Naidu Nerella, V., et al. (2018a). Effect of polypropylene fibre addition on properties of geopolymers made by 3D printing for digital construction. *Materials* 11, 2352. doi:10.3390/ma11122352

Nematollahi, B., Xia, M., Bong, S. H., and Sanjayan, J. (2018b). "Hardened properties of 3D printable 'one-part'geopolymer for construction applications," in *RILEM international conference on concrete and digital fabrication* (Berlin, Germany: Springer), 190–199. doi:10.1007/978-3-319-99519-9_17

Nematollahi, B., Xia, M., and Sanjayan, J. (2019a). Post-processing methods to improve strength of particle-bed 3D printed geopolymer for digital construction applications. *Front. Mater.* 6, 160. doi:10.3389/fmats.2019.00160

Nematollahi, B., Xia, M., Vijay, P., and Sanjayan, J. G. (2019b). "Properties of extrusion-based 3D printable geopolymers for digital construction applications," in *3D concrete printing technology* (Netherlands: Elsevier), 371–388. doi:10.1016/B978-0-12-815481-6.00018-X

Nerella, V. N., and Mechtcherine, V. (2019). "Studying the printability of fresh concrete for formwork-free concrete onsite 3D printing technology (CONPrint3D)," in *3D concrete printing technology* (Netherlands: Elsevier), 333–347. doi:10.1016/B978-0-12-815481-6.00016-6

Neupane, K. (2016). Fly ash and GGBFS based powder-activated geopolymer binders: a viable sustainable alternative of portland cement in concrete industry. *Mech. Mater.* 103, 110–122. doi:10.1016/j.mechmat.2016.09.012

Ngo, T. D., Kashani, A., Imbalzano, G., Nguyen, K. T., and Hui, D. (2018). Additive manufacturing (3D printing): a review of materials, methods, applications and challenges. *Compos. Part B Eng.* 143, 172–196. doi:10.1016/j.compositesb.2018.02.012

Pan, Z., Si, D., Tao, J., and Xiao, J. (2023). Compressive behavior of 3D printed concrete with different printing paths and concrete ages. *Case Stud. Constr. Mater.* 18, e01949. doi:10.1016/j.cscm.2023.e01949

Panda, B., Lim, J. H., and Tan, M. J. (2019a). Mechanical properties and deformation behaviour of early age concrete in the context of digital construction. *Compos. Part B Eng.* 165, 563–571. doi:10.1016/j.compositesb.2019.02.040

Panda, B., Mohamed, N., and Tan, M. J. (2019b). "Rheology and structural rebuilding of one-part geopolymer mortar in the context of 3D concrete printing," in *Rheology and processing of construction materials* (Berlin, Germany: Springer), 426–431. doi:10.1007/978-3-030-22566-7_49

Panda, B., Paul, S. C., Hui, L. J., Tay, Y. W. D., and Tan, M. J. (2017a). Additive manufacturing of geopolymer for sustainable built environment. *J. Clean. Prod.* 167, 281–288. doi:10.1016/j.jclepro.2017.08.165

Panda, B., Paul, S. C., Mohamed, N. N., Tay, Y. W. D., and Tan, M. J. (2018a). Measurement of tensile bond strength of 3D printed geopolymer mortar. *Measurement* 113, 108–116. doi:10.1016/j.measurement.2017.08.051

Panda, B., Paul, S. C., and Tan, M. J. (2017b). Anisotropic mechanical performance of 3D printed fiber reinforced sustainable construction material. *Mater. Lett.* 209, 146–149. doi:10.1016/j.matlet.2017.07.123

Panda, B., Singh, G. B., Unluer, C., and Tan, M. J. (2019c). Synthesis and characterization of one-part geopolymers for extrusion based 3D concrete printing. *J. Clean. Prod.* 220, 610–619. doi:10.1016/j.jclepro.2019.02.185

Panda, B., and Tan, M. J. (2018). Experimental study on mix proportion and fresh properties of fly ash based geopolymer for 3D concrete printing. *Ceram. Int.* 44, 10258–10265. doi:10.1016/j.ceramint.2018.03.031

Panda, B., and Tan, M. J. (2019). Rheological behavior of high volume fly ash mixtures containing micro silica for digital construction application. *Mater. Lett.* 237, 348–351. doi:10.1016/j.matlet.2018.11.131

Panda, B., Unluer, C., and Tan, M. J. (2018b). Investigation of the rheology and strength of geopolymer mixtures for extrusion-based 3D printing. *Cem. Concr. Compos.* 94, 307–314. doi:10.1016/j.cemconcomp.2018.10.002

Panda, B., Unluer, C., and Tan, M. J. (2019d). Extrusion and rheology characterization of geopolymer nanocomposites used in 3D printing. *Compos. Part B Eng.* 176, 107290. doi:10.1016/j.compositesb.2019.107290

Panda, B., Ruan, S., Unluer, C., and Tan, M. J. (2020). Investigation of the properties of alkali-activated slag mixes involving the use of nanoclay and nucleation seeds for 3D printing. *Compos. Part B Eng.* 186, 107826. doi:10.1016/j.compositesb.2020.107826

Pasupathy, K., Ramakrishnan, S., and Sanjayan, J. (2023). 3D concrete printing of eco-friendly geopolymer containing brick waste. *Cem. Concr. Compos.* 138, 104943. doi:10.1016/j.cemconcomp.2023.104943

Paul, S. C., Tay, Y. W. D., Panda, B., and Tan, M. J. (2018). Fresh and hardened properties of 3D printable cementitious materials for building and construction. *Archives Civ. Mech. Eng.* 18, 311–319. doi:10.1016/j.acme.2017.02.008

Perrot, A., Rangeard, D., and Pierre, A. (2016). Structural built-up of cement-based materials used for 3D-printing extrusion techniques. *Mater. Struct.* 49, 1213–1220. doi:10.1617/s11527-015-0571-0

Ranjbar, N., Kuenzel, C., Gundlach, C., Kempen, P., and Mehrali, M. (2023). Halloysite reinforced 3D-printable geopolymers. *Cem. Concr. Compos.* 136, 104894. doi:10.1016/j.cemconcomp.2022.104894

Ranjbar, N., Mehrali, M., Kuenzel, C., Gundlach, C., Pedersen, D. B., Dolatshahi-Pirouz, A., et al. (2021). Rheological characterization of 3D printable geopolymers. *Cem. Concr. Res.* 147, 106498. doi:10.1016/j.cemconres.2021.106498

Rehman, A. U., and Kim, J.-H. (2021). 3D concrete printing: a systematic review of rheology, mix designs, mechanical, microstructural, and durability characteristics. *Materials* 14, 3800. doi:10.3390/ma14143800

Roussel, N. (2018). Rheological requirements for printable concretes. *Cem. Concr. Res.* 112, 76–85. doi:10.1016/j.cemconres.2018.04.005

Şahin, O., İlcan, H., Ateşli, A. T., Kul, A., Yıldırım, G., and Şahmaran, M. (2021). Construction and demolition waste-based geopolymers suited for use in 3-dimensional additive manufacturing. *Cem. Concr. Compos.* 121, 104088. doi:10.1016/j.cemconcomp.2021.104088

Sanjayan, J. G., Nematollahi, B., Xia, M., and Marchment, T. (2018). Effect of surface moisture on inter-layer strength of 3D printed concrete. *Constr. Build. Mater.* 172, 468–475. doi:10.1016/j.conbuildmat.2018.03.232

Santos, T. A., Cilla, M. S., and Ribeiro, e. D. V. (2022). Use of asbestos cement tile waste (ACW) as mineralizer in the production of Portland cement with low CO2 emission and lower energy consumption. *J. Clean. Prod.* 335, 130061. doi:10.1016/j.jclepro.2021.130061

Sathvik, S., Shakor, P., Hasan, S., Awuzie, B. O., Singh, A. K., Rauniyar, A., et al. (2023). Evaluating the potential of geopolymer concrete as a sustainable alternative for thin white-topping pavement. *Front. Mater.* 10, 1181474. doi:10.3389/fmats.2023.1181474

Shakor, P., Gowripalan, N., and Rasouli, H. (2021). Experimental and numerical analysis of 3D printed cement mortar specimens using inkjet 3DP. *Archives Civ. Mech. Eng.* 21, 58–16. doi:10.1007/s43452-021-00209-3

Shakor, P., Nejadi, S., and Gowripalan, N. (2020a). "Effect of heat curing and E6-glass fibre reinforcement addition on powder-based 3DP cement mortar," in *Second RILEM international conference on concrete and digital fabrication: digital concrete* (Berlin, Germany: Springer), 508–515. doi:10.1007/978-3-030-49916-7_52

Shakor, P., Nejadi, S., and Paul, G. (2019a). A study into the effect of different nozzles shapes and fibre-reinforcement in 3D printed mortar. *Materials* 12, 1708. doi:10.3390/ma12101708

Shakor, P., Nejadi, S., Paul, G., and Gowripalan, N. (2023). Effects of different orientation angle, size, surface roughness, and heat curing on mechanical behavior of 3D printed cement mortar with/without glass fiber in powder-based 3DP. *3D Print. Addit. Manuf.* 10, 330–355. doi:10.1089/3dp.2021.0067

Shakor, P., Nejadi, S., Paul, G., and Malek, S. (2019b). Review of emerging additive manufacturing technologies in 3D printing of cementitious materials in the construction industry. *Front. Built Environ.* 4, 85. doi:10.3389/fbuil.2018.00085

Shakor, P., Nejadi, S., Sutjipto, S., Paul, G., and Gowripalan, N. (2020b). Effects of deposition velocity in the presence/absence of E6-glass fibre on extrusion-based 3D printed mortar. *Addit. Manuf.* 32, 101069. doi:10.1016/j.addma.2020.101069

Shakor, P., Renneberg, J., Nejadi, S., and Paul, G. (2017). "Optimisation of different concrete mix designs for 3D Printing by utilising 6DOF industrial robot," in *ISARC*

2017-proceedings of the 34th international symposium on automation and robotics in construction (Taipei, Taiwan: IAARC). doi:10.22260/ISARC2017/0036

Siddika, A., Mamun, M. a.A., Ferdous, W., Saha, A. K., and Alyousef, R. (2020). 3D-printed concrete: applications, performance, and challenges. *J. Sustain. Cement-Based Mater.* 9, 127–164. doi:10.1080/21650373.2019.1705199

Souza, M. T., Simão, L., De Moraes, E. G., Senff, L., De Castro Pessôa, J. R., Ribeiro, M. J., et al. (2021). Role of temperature in 3D printed geopolymers: evaluating rheology and buildability. *Mater. Lett.* 293, 129680. doi:10.1016/j.matlet.2021.129680

Sun, C., Xiang, J., Xu, M., He, Y., Tong, Z., and Cui, X. (2020). 3D extrusion free forming of geopolymer composites: materials modification and processing optimization. *J. Clean. Prod.* 258, 120986. doi:10.1016/j.jclepro.2020.120986

Tang, D., and Tang, H. (2022). Self-healing diamond/geopolymer composites fabricated by extrusion-based additive manufacturing. *Addit. Manuf.* 56, 102898. doi:10.1016/j.addma.2022.102898

Tay, C. H., and Norkhairunnisa, M. (2021). Mechanical strength of graphene reinforced geopolymer nanocomposites: a review. *Front. Mater.* 8, 661013. doi:10.3389/fmats.2021.661013

Tay, Y. W. D., Panda, B., Paul, S. C., Noor Mohamed, N. A., Tan, M. J., and Leong, K. F. (2017). 3D printing trends in building and construction industry: a review. *Virtual Phys. Prototyp.* 12, 261–276. doi:10.1080/17452759.2017.1326724

Uddin, M. N., Ye, J., Deng, B., Li, L.-Z., and Yu, K. (2023). Interpretable machine learning for predicting the strength of 3D printed fiber-reinforced concrete (3DP-FRC). *J. Build. Eng.* 72, 106648. doi:10.1016/j.jobe.2023.106648

Vlachakis, C., Perry, M., Biondi, L., and Mcalorum, J. (2020). 3D printed temperature-sensing repairs for concrete structures. *Addit. Manuf.* 34, 101238. doi:10.1016/j.addma.2020.101238

Wang, Y.-S., Alrefaei, Y., and Dai, J.-G. (2019). Silico-aluminophosphate and alkali-aluminosilicate geopolymers: a comparative review. *Front. Mater.* 6, 106. doi:10.3389/fmats.2019.00106

Wangler, T., Lloret, E., Reiter, L., Hack, N., Gramazio, F., Kohler, M., et al. (2016). Digital concrete: opportunities and challenges. *RILEM Tech. Lett.* 1, 67–75. doi:10.21809/rilemtechlett.2016.16

Wangler, T., Roussel, N., Bos, F. P., Salet, T. A., and Flatt, R. J. (2019). Digital concrete: a review. *Cem. Concr. Res.* 123, 105780. doi:10.1016/j.cemconres.2019.105780

Xia, M., Nematollahi, B., and Sanjayan, J. (2019). Printability, accuracy and strength of geopolymer made using powder-based 3D printing for construction applications. *Automation Constr.* 101, 179–189. doi:10.1016/j.autcon.2019.01.013

Xie, J., Wang, J., Rao, R., Wang, C., and Fang, C. (2019). Effects of combined usage of GGBS and fly ash on workability and mechanical properties of alkali activated geopolymer concrete with recycled aggregate. *Compos. Part B Eng.* 164, 179–190. doi:10.1016/j.compositesb.2018.11.067

Yang, H., Li, W., and Che, Y. (2020). The correlation between vitamin D receptor (vdr) gene polymorphisms and autism: a meta-analysis. *Front. Mater.* 7, 260–268. doi:10.1007/s12031-019-01464-z

Yuan, Q., Gao, C., Huang, T., Zuo, S., Yao, H., Zhang, K., et al. (2022). Factors influencing the properties of extrusion-based 3D-printed alkali-activated fly ash-slag mortar. *Materials* 15, 1969. doi:10.3390/ma15051969

Zhang, C., Nerella, V. N., Krishna, A., Wang, S., Zhang, Y., Mechtcherine, V., et al. (2021). Mix design concepts for 3D printable concrete: a review. *Cem. Concr. Compos.* 122, 104155. doi:10.1016/j.cemconcomp.2021.104155

Zhang, D.-W., Wang, D.-M., Lin, X.-Q., and Zhang, T. (2018). The study of the structure rebuilding and yield stress of 3D printing geopolymer pastes. *Constr. Build. Mater.* 184, 575–580. doi:10.1016/j.conbuildmat.2018.06.233

Zhang, J., Wang, J., Dong, S., Yu, X., and Han, B. (2019). A review of the current progress and application of 3D printed concrete. *Compos. Part A Appl. Sci. Manuf.* 125, 105533. doi:10.1016/j.compositesa.2019.105533

Zhao, J., Tong, L., Li, B., Chen, T., Wang, C., Yang, G., et al. (2021). Eco-friendly geopolymer materials: a review of performance improvement, potential application and sustainability assessment. *J. Clean. Prod.* 307, 127085. doi:10.1016/j.jclepro.2021.127085

Zhong, J., Zhou, G.-X., He, P.-G., Yang, Z.-H., and Jia, D.-C. (2017). 3D printing strong and conductive geo-polymer nanocomposite structures modified by graphene oxide. *Carbon* 117, 421–426. doi:10.1016/j.carbon.2017.02.102

Zhou, G.-X., Li, C., Zhao, Z., Qi, Y.-Z., Yang, Z.-H., Jia, D.-C., et al. (2020). 3D printing geopolymer nanocomposites: graphene oxide size effects on a reactive matrix. *Carbon* 164, 215–223. doi:10.1016/j.carbon.2020.02.021